Deep-Space Calibration of the WindSat Radiometer

W. Linwood Jones, *Fellow, IEEE*, Jun D. Park, *Student Member, IEEE*, Seubson Soisuvarn, *Student Member, IEEE*, Liang Hong, *Student Member, IEEE*, Peter W. Gaiser, *Senior Member, IEEE*, and Karen M. St. Germain, *Senior Member, IEEE*

***Abstract*—The WindSat microwave polarimetric radiometer consists of 22 channels of polarized brightness temperatures operating at five frequencies: 6.8, 10.7, 18.7, 23.8, and 37.0 GHz. The 10.7-, 18.7-, and 37.0-GHz channels are fully polarimetric (vertical/horizontal, $\pm 45^\circ$ and left-hand and right-hand circularly polarized) to measure the four Stokes radiometric parameters. The principal objective of this Naval Research Laboratory experiment, which flys on the USAF Coriolis satellite, is to provide the proof of concept of the first passive measurement of ocean surface wind vector from space. This paper presents details of the on-orbit absolute radiometric calibration procedure, which was performed during of a series of satellite pitch maneuvers. During these special tests, the satellite pitch was slowly ramped to $+45^\circ$ (and -45°), which caused the WindSat conical spinning antenna to view deep space during the forward (or aft portion) of the azimuth scan. When viewing the homogeneous and isotropic brightness of space (2.73 K) through both the main reflector and the cold-load calibration reflector, it is possible to determine the absolute calibration of the individual channels and the relative calibration bias between polarimetric channels. Results demonstrate consistent and stable channel calibrations (with very small brightness biases) that exceed the mission radiometric calibration requirements.**

***Index Terms*—Calibration, radiometer, WindSat.**

I. Introduction

WINDSAT is the world's first microwave polarimetric radiometer in space, and the principal sensor on the Coriolis satellite that was launched into a nearly polar, sun-synchronous, low Earth orbit on January 6, 2003. The mission objective is to demonstrate the "proof of concept" of a new microwave polarimetric radiometry technique for measuring the ocean surface wind vector (speed and *direction*) from space. The WindSat was designed, built, and tested at the Naval Research Laboratory (NRL) in Washington, DC, under sponsorship from the U.S. Navy and the National Polar-orbiting Operational Environmental Satellite System (NPOESS) Integrated Program Office.

Manuscript received February 7, 2005; revised June 13, 2005. This work was supported by the Naval Research Laboratory WindSat Program.

W. L. Jones, S. Soisuvarn, and L. Hong are with the Electrical and Computer Engineering Department, University of Central Florida, Orlando, FL 32816 USA (e-mail: ljones5@cfl.rr.com; se867731@pegasus.cc.ucf.edu; li413535@ucf.edu).

J. D. Park was with University of Central Florida, Orlando, FL 32825 USA. He is now with Northrop Grumman Corporation, Winter Park, FL 32789 USA (e-mail: jpark@mail.ucf.edu).

P. W. Gaiser is with Naval Research Laboratory, Washington, DC 20375 USA (e-mail: peter.gaiser@nrl.navy.mil).

K. M. St. Germain is with the National Polar-orbiting Operational Environmental Satellite System Integrated Program Office, National Oceanic and Atmospheric Administration, Silver Spring, MD 20910 USA (e-mail: Karen.StGermain@noaa.gov).

Digital Object Identifier 10.1109/TGRS.2005.862499

The WindSat system presents several unique radiometric calibration challenges because the ocean wind direction signal is two orders of magnitude smaller than the geophysical signals typically measured by passive microwave imagers. As such, the design sensitivity analysis resulted in sensor noise and absolute accuracy requirements approximately 50% tighter than the current Special Sensor Microwave Imager (SSM/I) operational performance [1]. Antenna and receiver polarization purity and horn/antenna/payload alignments are significant elements of the accuracy error budget, and the requirements for radiometric calibration are especially stringent because this is the first polarimetric radiometer to fly in space, and this mission also serves as a risk-reduction pathfinder for the polarimetric channels on the future NPOESS Conical Scanning Microwave Imager/Sounder (CMIS) instrument.

This paper provides a brief description of the WindSat instrument from the standpoint of brightness temperature (Tb) measurement calibration. Results are presented for special on-orbit radiometric calibration tests that include: 1) a special pitch maneuver whereby the spacecraft is adjusted in pitch to cause the spinning antenna to view space, and 2) measurements to assess the spillover of the main reflector during the cold-load calibration. Other aspects of the system calibration and engineering performance are discussed in a series of papers [1]–[3], but this paper focuses on radiometric calibration dealing with the multibeam antenna including both component beams produced by the main reflector and the secondary cold-sky reflector.

A. WindSat Instrument Overview

The WindSat is a conical passive microwave imager similar to the SSM/I [4] that operates on the U.S. Air Force's Defense Meteorological Support Program (DMSP) polar, low Earth orbit, weather satellites. SSM/I makes measurements over a single forward-looking (or aft-looking, depending upon the satellite configuration) swath. On the other hand, WindSat has two separate swaths: a forward-look ($\sim \pm 60^\circ$ about the subsatellite ground track) and a reduced swath aft-look (azimuths 120° to 180°). This measurement geometry was implemented to test both the single-look and two-look wind vector retrieval techniques. This multifrequency microwave radiometer operates in discrete bands at 6.8, 10.7, 18.7, 23.8, and 37.0 GHz. The 10.7-, 18.7-, and 37.0-GHz channels are fully polarimetric [vertical/horizontal (V/H), $\pm 45^\circ$ and left-hand (LHCP) and right-hand circularly polarized (RHCP)], and the 6.8- and 23.8-GHz channels are dual polarized only (vertical and horizontal).

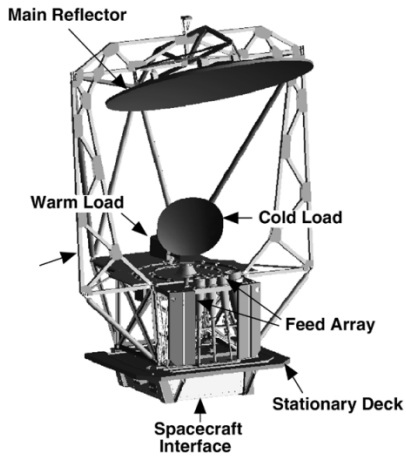

Fig. 1. Relevant components of the WindSat instrument involved in radiometric calibration.

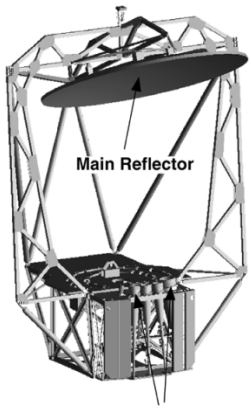

Fig. 2. WindSat antenna rotating assembly.

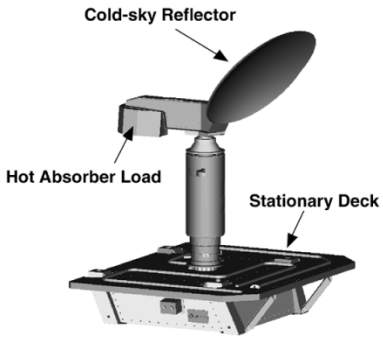

Fig. 3. WindSat calibration load nonrotating assembly.

A drawing of the WindSat instrument, shown in Fig. 1, illustrates the key radiometric components involved in the brightness temperature measurement. During the conical scan, the entire antenna/feed assembly (Fig. 2) rotates as a unit, and the stationary hot-load and cold-sky reflectors (Fig. 3) are viewed as the individual 11 feeds pass beneath them. The WindSat receivers are total-power radiometers, which view hot/cold calibration targets once per scan. The hot-load calibration is provided by a microwave absorber (blackbody) target (Fig. 4), and details of the design and on-orbit performance are presented in [2].

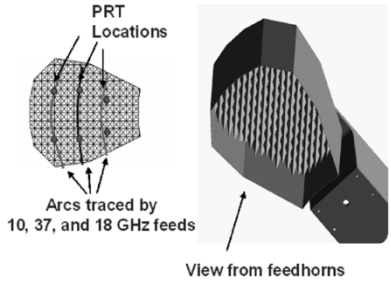

Fig. 4. Hot-load blackbody absorber assembly.

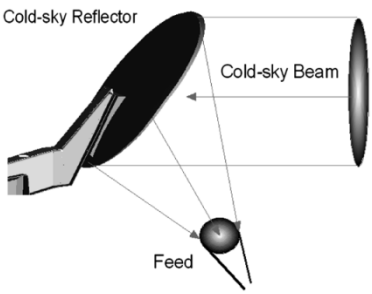

Fig. 5. WindSat cold-sky reflector (cold load) configuration. Eleven feeds sequentially move beneath the stationary reflector and form beams that view space.

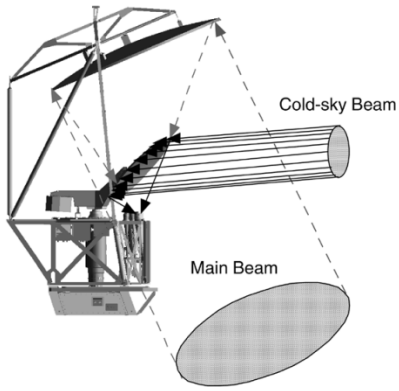

Fig. 6. Configuration of the cold-sky and main reflector beams during the cold-load measurement. The cold-sky reflector occults the main reflector when the feed is located near its focal point.

The cold-load target is a secondary cold-sky reflector that views the constant 2.73-K brightness of space (Fig. 5). During a portion of the azimuth scan, each feed passes beneath this offset parabolic reflector and a beam is formed that is directed toward space (Fig. 6). Because the cold-sky reflector occludes the main reflector, it blocks the energy collected by the main reflector from being collected by the feeds. Further, because each feed has a different displacement from the cold-sky reflector focal point, the beams are squinted-off of the reflector boresight (in the elevation plane) as shown in Fig. 7. In this figure, the satellite is over the South Pole and the cold-sky beams are passing through the equatorial plane. At every position in orbit, all beams point to space with negligible Earth interception.

A diagram, illustrating the scan sectors for forward and aft surface viewing, hot-load and cold-load measurements, is shown in Fig. 8. This diagram is not to scale as the exact

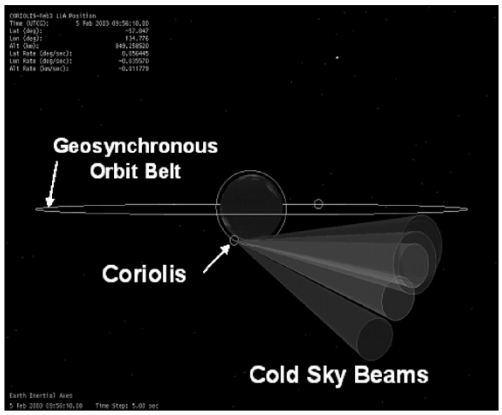

Fig. 7. Cold-sky reflector component beams that continuously view space.

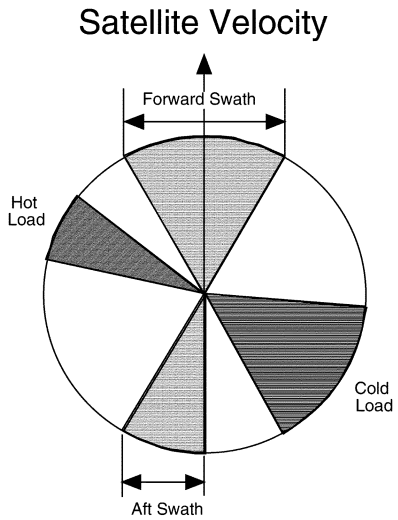

Fig. 8. Azimuthal distribution of WindSat measurement sectors.

azimuth angles for a given scan sector varies with the individual feeds (frequency and polarization).

B. Coriolis Pitch Maneuver

Over approximately 15 months, eight radiometric calibration procedures were successfully performed to assess the WindSat calibration repeatability. This procedure involved performing Tb measurements while the satellite's attitude was slowly varied in pitch to cause the antenna beams to point to space where the absolute brightness is a constant. Based upon observations from the National Aeronautics and Space Administration's (NASA) Cosmic Background Explorer (COBE) operating at 31, 53, and 90 GHz, space provides a uniform brightness temperature of 2.73 K with a variation of not more than 100 μK about the Galactic plane.[1] WindSat measurements were performed with the instrument in normal operational mode (i.e., antenna spinning and Tb sampling with both fore and aft viewing). The limit of the pitch bias was 45°, which caused the antenna to alternately view deep space or the ocean at near-nadir incidence respectively for azimuth positions of 0° (looking forward) and 180° (looking aft). Alternate maneuvers were performed which caused the satellite pitch to ramp in the opposite direction (negative pitch), and the azimuth direction for viewing space and ocean were reversed. With both positive and negative maneuvers, the main beam viewed space over the full operating azimuth ranges for fore and aft looks.

The next section gives a brief review of previous on-orbit calibrations of microwave radiometers. This is followed by a discussion of the WindSat calibration requirements; and finally, results are presented for the analysis of two different sets of on-orbit calibration measurements.

II. Background

A. Previous On-Orbit Pitch Maneuvers

In the late 1980s, the concept of using a satellite pitch maneuver for absolute radiometric calibration was first proposed by Hollinger [4] and later Jones [5] for the Low Frequency Microwave Radiometer (LFMR) on the Naval Remote Ocean Sensing System (NROSS). Because the NROSS program was cancelled, this on-orbit calibration procedure never occurred until 1998 on the Tropical Rainfall Measuring Mission (TRMM) spacecraft, and then it was fortuitous. In January 1998 and again in September 1998, as part of the Clouds and Earths Radiant Energy System (CERES) instrument calibration, TRMM was rotated in pitch by 180° so that the Earth-facing panel viewed deep space during several orbits. While this procedure was not intended for the benefit of the TRMM Microwave Imager (TMI), these maneuvers nevertheless proved to be extremely useful for calibrating TMI and for confirming the other two calibration methods developed by Wentz *et al.* [6].

The TMI is a slightly modified SSMI, which has a larger reflector antenna and two additional dual-polarized 10.69-GHz channels. As such, the system normally imaged the Earth's surface; however, when the TRMM pitched by 180°, then the TMI main reflector was pointed to a homogeneous and isotropic deep space at known absolute brightness of 2.73 K. In this manner, biases in the measured Tb, as well as variations in Tb with antenna azimuth position, were very apparent. The observed Tb errors were remarkably consistent with the results of two other traditional postlaunch calibration techniques: namely, statistical analysis of TMI ocean observations and an intercomparison of TMI and SSMI nearly simultaneous, collocated Tb observations. Therefore, the success of the first on-orbit pitch maneuver radiometric calibration on TRMM proved to be a valuable tool for future spaceborne radiometer systems.

B. SSMI Radiometric Intercomparisons

An extensive intercomparison of SSMI Tb measurements, for eight instruments over a decade of on-orbit operations, was performed by Colton and Poe [7]. This comprehensive study used statistical analysis of intersecting radiometer swaths and monthly averaged ocean Tbs to quantify the incremental brightness temperature differences to which the SSMIs can be intercalibrated. Sensor-specific components, orbital configuration, and systematic relative errors all contribute to the total system calibration.

Their studies have shown the presence of an along-scan asymmetry (1–2 K) associated with a pixel-dependent energy loss,

[1]http://aether.lbl.gov/www/projects/cobe/COBE_home/cobe_home.html

TABLE I
PITCH MANEUVER CALIBRATION MATRIX

Requirement	Deep Space + 45° Pitch	Nadir View - 45° Pitch
Main Reflector Reflectivity	Yes	
Cold-sky reflector -- Earth Bias	Yes	
Receiver Channel Biases	Yes	Yes
Absolute Tb Calibration	Yes	
Tb Along-scan Biases		
Forward Swath	Yes	
Aft Swath		Yes
Cold/Hot Load Blockage	Yes	Yes
NEDT	Yes	

most notable at the end of scan. The reason was explained to be an antenna field-of-view intrusion by the spacecraft and other sensors on DMSP. These effects were found to be correctable to first order using a pixel-dependent spillover correction. The root mean square (rms) errors associated with monthly averaged ocean Tbs limited the intersensor comparisons. Also, sensor-specific antenna pattern correction (APC) coefficients caused large differences, which were dramatically reduced when analyzed on the basis of the temperature data record (prior to applying the APC). They determined that SSMIs were intercalibrated at the TDR level to within the uncertainties of the methodology, namely, 0.25–0.35 K for the low-frequency channels and 0.45 K for the 85-GHz channels.

Further, they concluded that to acquire high intersensor accuracy, a single set of APC coefficients should be used. These should be derived from a full and accurate characterization of the feedhorn spillover loss and cross-polarization coupling to calculate the magnitude of the Sensor Data Record (SDR) radiometric biases. Reducing the Tb uncertainty noise floor to 0.1 K for future sensors will require highly detailed information about the sensor, improved orbital elements, and spacecraft attitude information.

C. AMSR-E On-Orbit Calibration

The Advanced Microwave Scanning Radiometer-EOS (AMSR-E) is one of the six sensors aboard NASA's Earth Observing System (EOS) Aqua satellite launched in May 2002. During the postlaunch calibration of the AMSR-E [8], it was reported that a significant radiometric calibration issue existed due to a hardware problem with the total-power radiometer hot-load calibration source. The problem resulted from the design of the microwave absorber blackbody target and the thermal control system. Because of random physical temperature gradients caused by independent heater thermostats, there was significant unknown variability in the brightness temperature of the high-temperature noise source (HTS). Because of this nonuniform blackbody temperature characteristic, the use of a simple two-point (hot/cold) calibration was not sufficient. An empirical calibration was performed using eight platinum resistance thermometers (PRTs) to get an approximate Teff, which was intercompared with collocated SSMI data. These analyses established an empirical relationship between receiver temperature and its gain variation, which allowed the absolute calibration to be established.

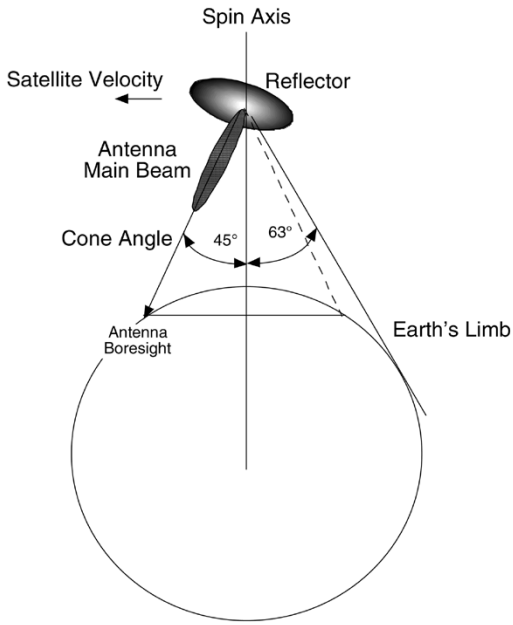

Fig. 9. WindSat normal conical-scanning measurement geometry.

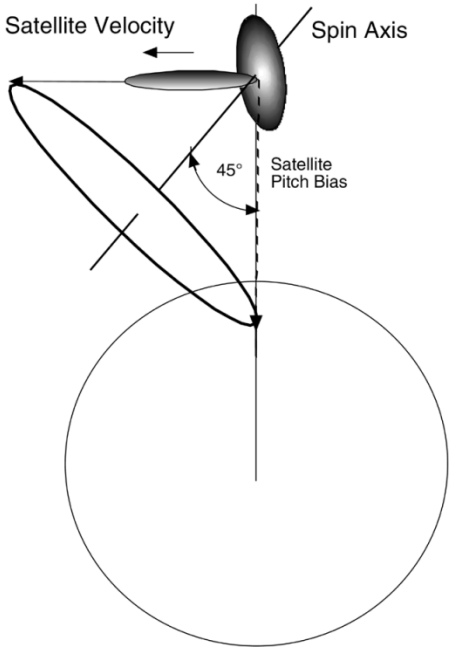

Fig. 10. WindSat conical-scanning measurement geometry during satellite pitch maneuver.

Further, there was a suspected spillover occurring between the feedhorn and Cold Sky Mirror (CSM) during the cold-load measurement. This caused an Earth radiance bias of $\sim$2 K in the 6-GHz channels; but fortunately, other channels were affected to a lesser amount. An adjustment spillover factor of around 0.4% was applied in correction. Also, along scan Tb biases ($\sim$1 K) were observed which resulted in systematic degradation of Tb at the beginning of the scan.

III. RADIOMETRIC CALIBRATION

The WindSat system presents several unique calibration and validation challenges because this instrument serves as the

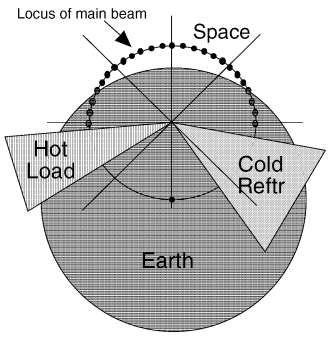

Fig. 11. Locus of main beam pointing into space during the positive 45° pitch maneuver. Also shown are the azimuth blockage ranges for the hot and cold calibration loads.

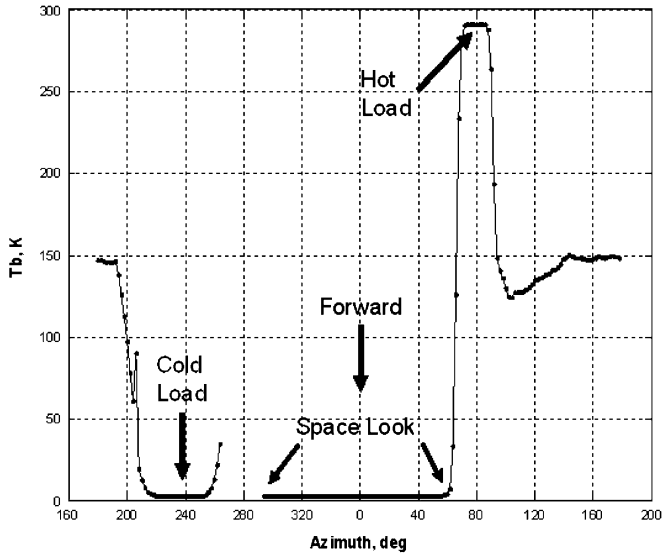

Fig. 12. Typical measured Tb (18 GHz), during a $+45°$ pitch maneuver. Forward measurement swath covers azimuth angles from approximately 290° to 50° (exact azimuth range is dependent upon individual feeds).

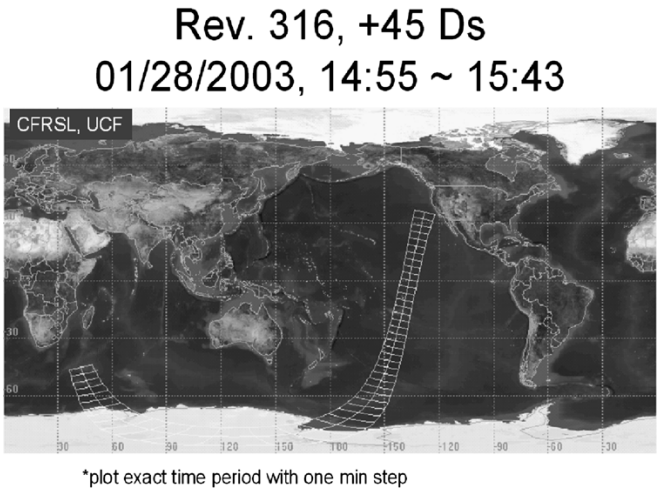

Fig. 13. Ground track for first WindSat $+45°$ pitch maneuver for descending rev-316 on January 28, 2003. Note that the satellite travels from North America to the South Pole.

proof-of-concept mission for the polarimetric radiometry technique for measuring oceanic wind vector. The wind direction dependence of the third and fourth Stokes parameters is two

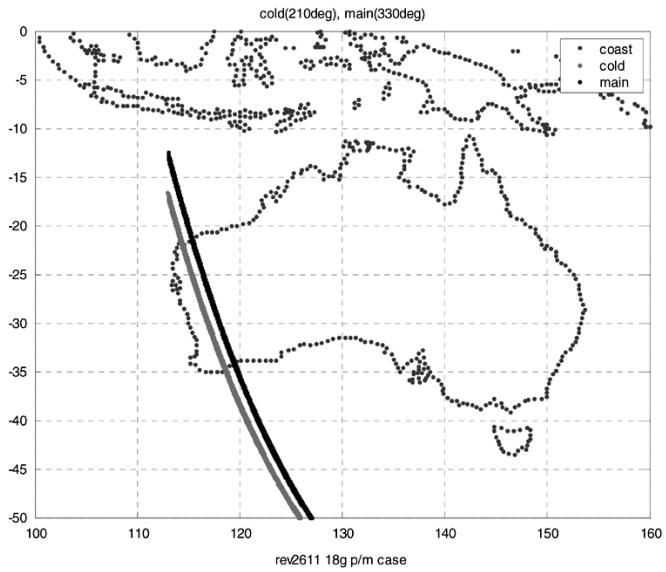

Fig. 14. Typical ground track for the main reflector during the cold-load measurement ($\sim 210°$, gay line) and while viewing forward at the right-hand swath edge ($\sim 330°$, black line). Satellite orbit, rev-2611, is ascending from south to north.

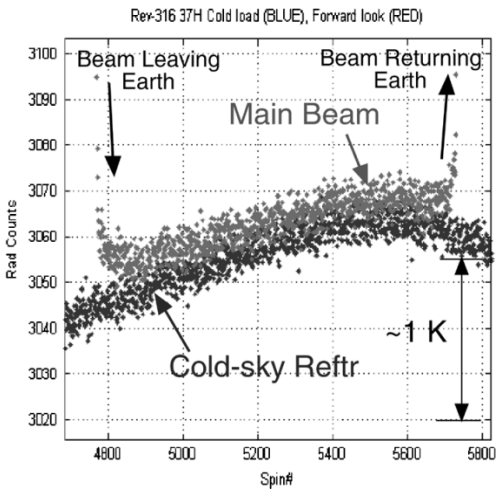

Fig. 15. Radiometer output (rad_counts) during pitch maneuver, rev-316, for main beam forward look (light gray) and cold-sky reflector (dark gray) for 37-GHz H-pol. The X axis is spin number (relative time).

orders of magnitude smaller than the vertical and horizontal polarization signals typically measured by passive microwave imagers. As such, the design sensitivity analysis resulted in sensor noise and absolute accuracy requirements approximately 50% tighter than the current SSM/I operational performance. Antenna and receiver polarization purity and horn/antenna/payload alignments are significant elements of the accuracy error budget. Also, the requirements for radiometric calibration are especially stringent because this is the first polarimetric radiometer to fly in space and this mission serves as a risk-reduction pathfinder for the polarimetric channels on the future NPOESS CMIS instrument; therefore extreme care was made to provide the purest absolute calibration for the radiometer channels. In this way, it should be possible to separate instrumental effects from geophysical effects, which is vital for application to other instrument designs such as CMIS.

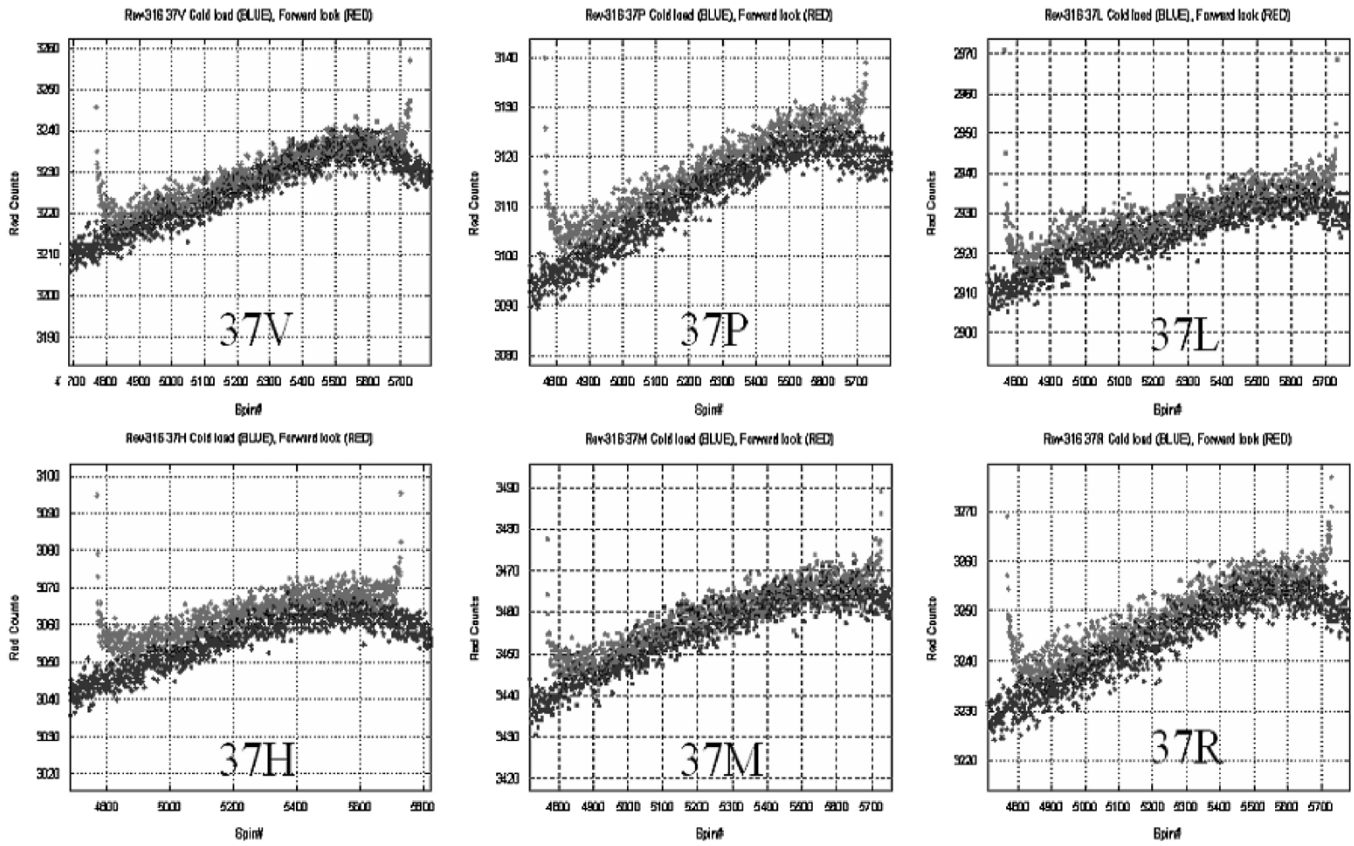

Fig. 16. Time series of radiometer output (rad_counts) during positive pitch maneuver, rev-316, for main beam forward look (light gray) and cold-sky reflector (dark gray) for 37 GHz all polarizations: V = vertical, H = horizontal, $P = +45°$, $M = -45°$, L = left-hand circular and R = right-hand circular. The X axis is spin number (relative time).

A. Calibration Requirements

To satisfy these objectives, a detailed calibration study was conducted prelaunch to define the requirements and recommended procedure to be used postlaunch. The key calibration requirements from this study are summarized in Table I. Early on, it was identified that on-orbit calibration would involve brightness temperature measurements of selected distributed Earth targets and deep space. These measurements were to be performed with the instrument in normal operational mode (i.e., antenna spinning and sampling with both fore and aft viewing surface brightness temperatures). Further, the majority of these requirements could be satisfied during a special spacecraft pitch maneuver used to assess the WindSat instrument radiometric calibration accuracy and stability. In addition, this on-orbit testing could be used to perform other engineering evaluations of the radiometer system to characterize its end-to-end radiometric performance while operating in its orbital environment.

B. Satellite Pitch Maneuver

WindSat on-orbit calibration testing commenced during special satellite pitch maneuvers in January 2003, which occurred after preliminary engineering tests were completed and the satellite reached a stable orbit. WindSat operated in the normal spinning mode, and brightness temperature measurements were performed while the satellite pitch increased from a normal nadir-pointing attitude (Fig. 9) to a $+45°$ pitched-up attitude (Fig. 10). In this special attitude control mode, the satellite pitch was slowly ramped at approximately 0.035°/s until the pitch reached 45°, after which it was held constant for 10 min and then ramped down to the nominal 0° pitch operational attitude. From Fig. 9, the WindSat antenna looking forward (azimuth $= 0°$) viewed the Earth's limb (tangency point) when the satellite pitch reached 18°. As the satellite pitch increased, the antenna beam scanned off the surface of the Earth to repeatedly view deep space over a portion of each antenna revolution.

Fortunately, at WindSat frequencies, space is a homogeneous, isotropic distributed target of constant brightness $2.73\ \text{K} \pm 100\ \mu\text{K}$ determined by NASA's COBE observations. This greatly simplified the radiometric calibration procedure by not requiring an adjustment in the observed brightness temperature depending on the pointing direction into space; but of course, the main beam pointing toward both the moon and sun were avoided. During the $+45°$ pitch dwell period, the antenna beam for the entire forward scan was located off the Earth as shown in Fig. 11. A typical plot of the measured Tb versus azimuth is shown in Fig. 12 for the 18-GHz M-pol $(-45°)$ channel. When the main beam views space, the brightness temperature is 2.73 K. This occurs over the azimuth range of approximately 290° to 60° relative to the satellite velocity, which is the azimuth range over which the antenna has a clear field of view of the ocean surface. Beyond this azimuth range are the locations of the radiometer calibration targets: hot-load microwave absorber and the cold-sky reflector.

While the main reflector viewed space, all of WindSat's 11 feeds (22 beams or channels) viewed a constant 2.73-K

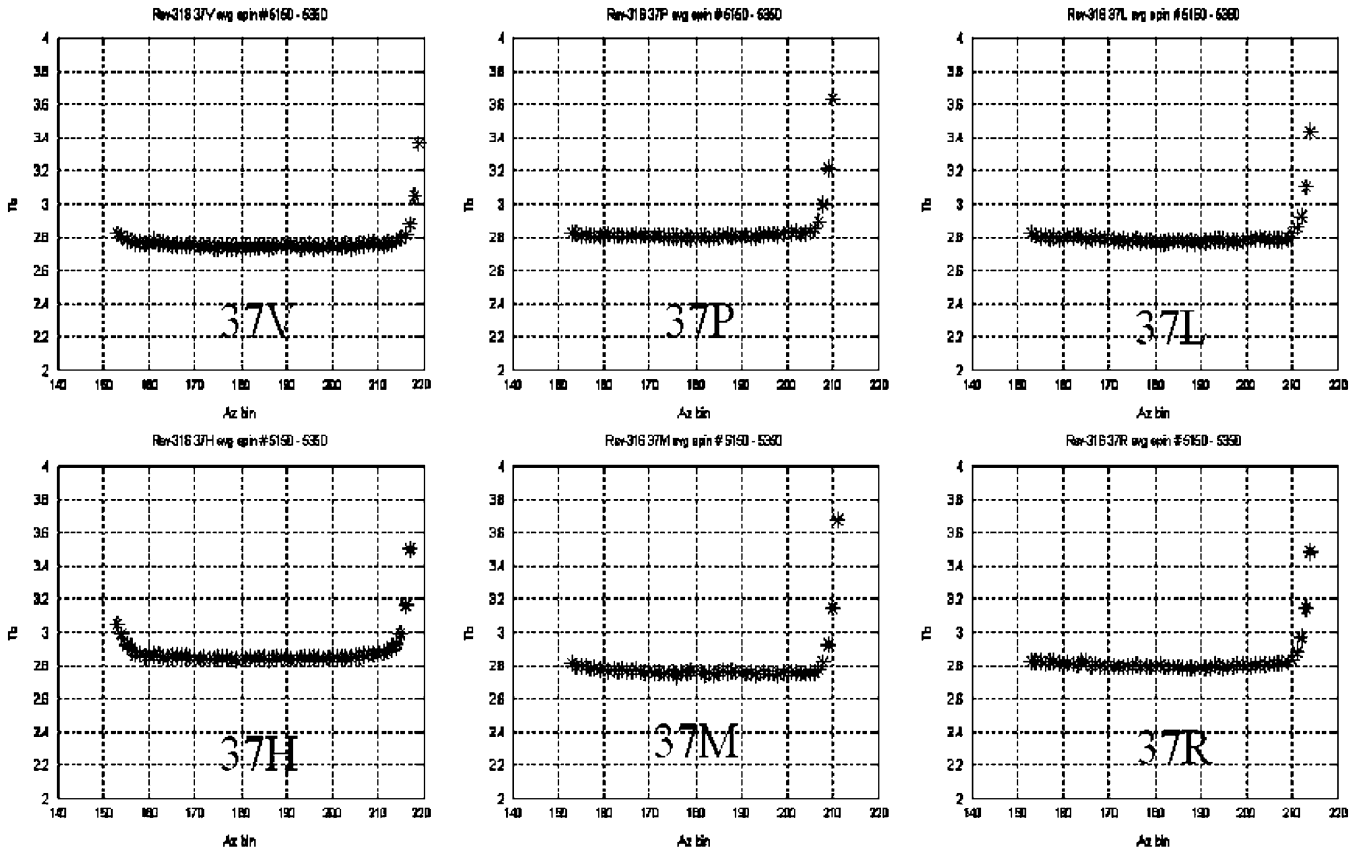

Fig. 17. Measured azimuthal distribution of main reflector Tb (forward look) during $+45^\circ$ pitch dwell, rev-316, for 37 GHz all polarizations. The X axis is azimuth bin number (2° steps) where number $180 = 360^\circ$ and bin number <180 view to the left side of the satellite subtrack and bin number >180 view to the right.

nonpolarized brightness, i.e., all polarizations were equal. Each radiometer channel measured a single-polarization brightness temperature using independent receivers, detectors, and integrators. While viewing space, comparisons were made between orthogonal polarized radiometer channels to assure that no radiometric biases existed that could affect the Stokes parameter measurements. Because the third and fourth Stokes parameters are zero-mean signals, channel biases, for the $\pm 45^\circ$ and LHCP/RHCP polarizations, must be determined very accurately (typically < 0.1 K) and removed during ground data processing. Also, comparisons were made between the energy collected by the main reflector and the cold-sky reflector, since differences in the reflection coefficient of these dishes can cause biases in the calculated Tb if not properly adjusted. During the pitch maneuver both reflectors view space nearly simultaneously. Therefore, the differences in the corresponding digitized radiometer output (known as "rad_counts") can be used to determine the differential reflectivity. Also, since the energy collected by the feed is constant, the radiometer measurement precision (delta-T) can be determined from the standard deviation of the radiometer output during space measurements.

A diagram of the satellite ground track for the first pitch maneuver (revolution-316) is shown in Fig. 13. The maneuver started as the satellite descended from the west coast of the U.S. and moved across the Pacific toward the South Pole. By the time the satellite crossed the equator, the satellite pitch was $\sim 18^\circ$ and the main beam first viewed space. For the next 12 min, the pitch increased until it reached the maximum value $(+45^\circ)$, where it remained for 10 min. While the forward portion of the azimuth scan $(\pm 60^\circ)$ viewed space, the aft portion at azimuth 180° viewed the ocean's surface at nadir. After the pitch dwell period, the satellite's pitch ramped down, and the main beam returned to the Earth's surface over Antarctica. The total duration of the maneuver was approximately 50 min ($\sim$ one-half an orbit). The initial satellite pitch maneuvers were over the Pacific Ocean where the Earth presented a well-characterized brightness temperature with no land in the WindSat antenna view. During the calibration/validation period, a total of eight pitch maneuvers were conducted for both positive and negative pitch, and most occurred over the Pacific Ocean except two, which occurred over land.

C. Cold-Calibration Spillover

During the postlaunch calibration of the AMSR-E [8], it was reported that coupling between the main reflector and the antenna feeds occurred during the cold-load measurement, which caused an Earth radiance bias of ~ 2 K in the 6-GHz channels. The coupling effects at other frequencies were less; as a result, other channels were affected to a lesser amount. Thus, to assess whether or not a similar impact existed on the WindSat radiometric calibration, an analysis was performed of cold-load brightness temperatures to calculate the coupling (spillover) between the main reflector and the 11 feeds (22 channels).

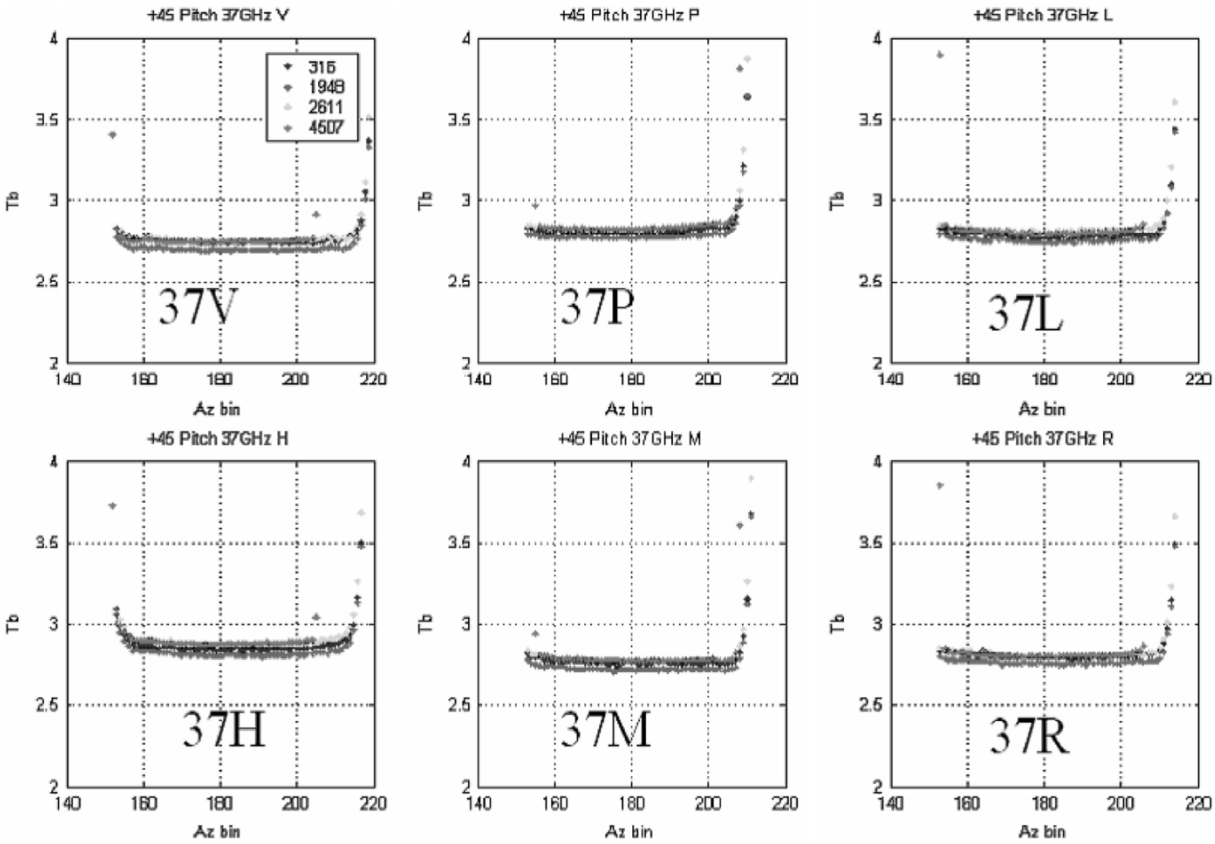

Fig. 18. Composite main reflector Tb for forward look during $+45^\circ$ pitch dwell for 37 GHz all polarizations for revs: 316, 1948, 2611, and 4607. The X axis is azimuth bin number (2° steps) where number $180 = 360^\circ$ and bin number <180 view to the left side of the satellite subtrack and bin number >180 view to the right.

TABLE II
MEAN/STANDARD DEVIATION BRIGHTNESS TEMPERATURE BIASES BETWEEN MAIN REFLECTOR AND COLD-SKY REFLECTOR FOR FORWARD AND AFT VIEWING

MAIN REFTR - 2.73K	V-Pol	H-Pol	+45-Pol	-45-Pol	L-Pol	R-Pol
6.8	0.09 K/ 0.05 K	0.11 K/ 0.04 K	N/A	N/A	N/A	N/A
10.7	0.05 K/ 0.05 K	0.06 K/ 0.03 K	0.09 K/ 0.03 K	0.08 K/ 0.04 K	0.08 K/ 0.04 K	0.06 K/ 0.04 K
18.7	-0.01 K/ 0.03 K	0.02 K/ 0.19 K	0.06 K/ 0.07 K	-0.03 K/ 0.30 K	0.03 K/ 0.04 K	0.02 K/ 0.08 K
23.8	0.09 K/ 0.12 K	0.10 K/ 0.05 K	N/A	N/A	N/A	N/A
37.0	0.05 K/ 0.03 K	0.16 K/ 0.03 K	0.12 K/ 0.03 K	0.07 K/ 0.03 K	0.10 K/ 0.02 K	0.10 K/ 0.02 K

During the cold-load measurement, the stationary cold-sky reflector occludes the counterclockwise rotating main reflector and the feed/cold-sky reflector forms a beam that views the homogeneous and isotropic 2.73-K brightness of space. This occurs at an antenna azimuth position of $\sim 210^\circ$, while the main reflector simultaneously views the Earth's surface (looking aft and to the right-hand side of the satellite subtrack). Since spillover of the main reflector brightness can result, to prevent degradation of the cold-load reference temperature, the magnitude of this coupling must be negligibly small (typically < -30 dB); or if greater, the coupling must be precisely known to allow for a bias subtraction.

A number of different measurement scenarios were examined; but the most reliable results were obtained by examining the cold-load rad_counts [raw data record (RDR)] while the satellite passed over large nearly homogeneous landmasses surrounded by ocean. For this analysis, five passes over Australia and one over South America were selected during the period April–July, 2003. The ground track is presented, for one of the cases in Fig. 14, an ascending pass over Australia. To estimate the corresponding main reflector brightness during the cold-load measurement, a time series of radiometer measurements through the main reflector was produced for the right-hand edge of scan while viewing forward. This path taken by the main beam on the surface (black trace) is the closest to the locus of main reflector swath looking aft (gray trace), which occurred during the azimuth position corresponding to the cold-load measurement (cold-sky reflector "sweet-spot"). After adjusting for the time difference in the main reflector and the cold-load measurements, the time series were cross-correlated to establish the coupling.

IV. RESULTS

A. $+45^\circ$ *Pitch Maneuvers*

The analysis of the pitch maneuver radiometric calibration verified that the absolute calibration accuracy for the 22 channels far exceeded the system requirements. Over approximately

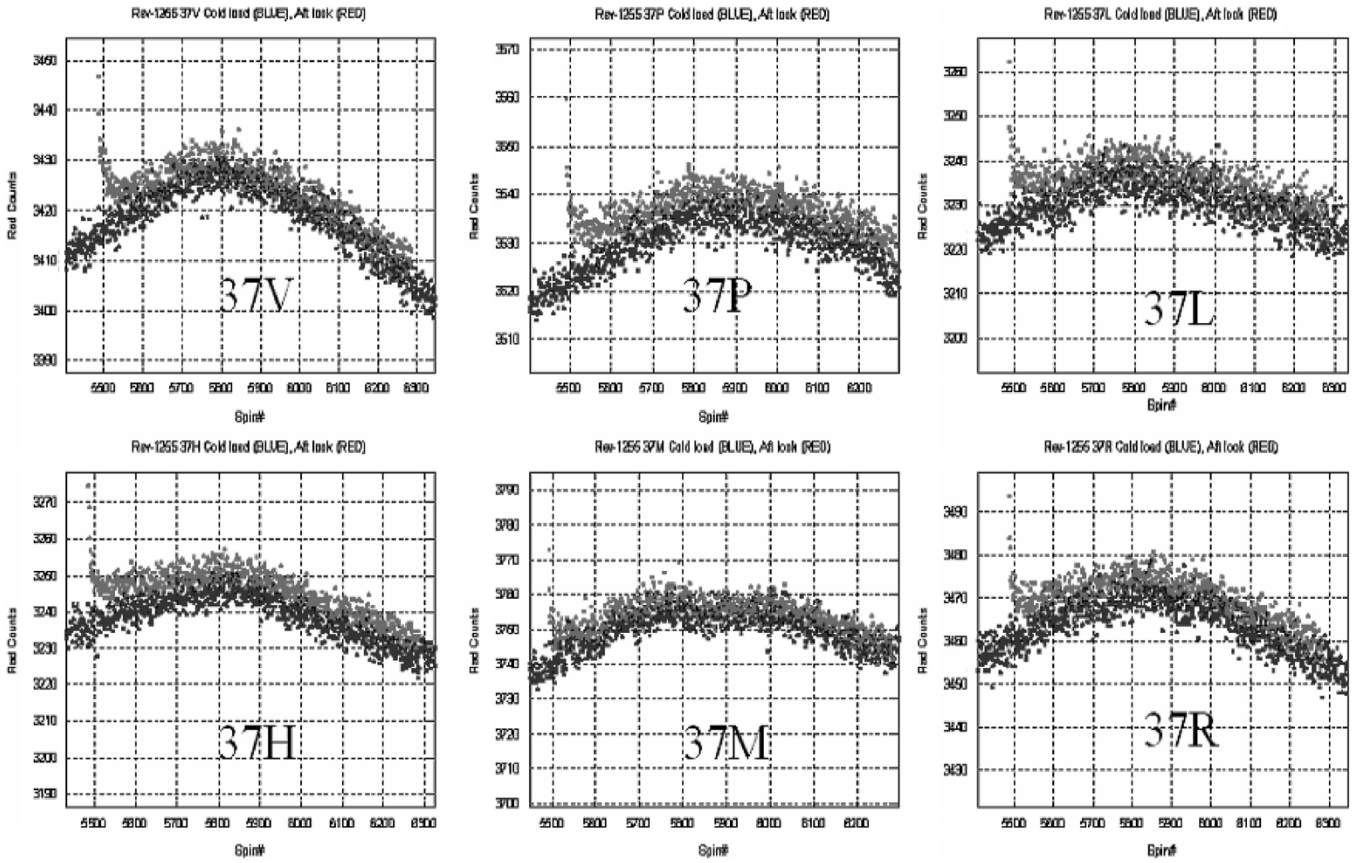

Fig. 19. Time series of radiometer output (rad_counts) during negative pitch maneuver, rev-1255, for main beam aft look (light gray) and cold-sky reflector (dark gray) for 37 GHz all polarizations. The X axis is spin number (relative time).

15 months, eight maneuvers were performed (positive and negative pitch) to assess the calibration repeatability, which was excellent. Initially, tracks were chosen over the Pacific Ocean to provide a cold ocean background for antenna sidelobes, while the main beam viewed space. Later calibrations were performed over land, with little to no effect observed.

While viewing space, the "raw" (uncalibrated) radiometer output voltage (rad_counts) for the component beams (secondary patterns from the main reflector) were compared to the respective cold-sky calibration reflector measurements to establish the absolute radiometric bias of the main beam as a function of the azimuth viewing direction. Results for all channels were very similar; and an example of the forward azimuth look for Coriolis orbit number (or revolution, rev) 316 is presented in Fig. 15. In this figure, the 37-GHz H-pol rad_counts are plotted versus time (spin number) during this $+45^\circ$ pitch maneuver. The main beam leaves the Earth's surface at spin number 4780 (as noted by the rapid decrease of main beam rad_counts, which are shown in light gray). The main beam continues to view space until spin number 5750 and after which it returns to the Earth. The period of space viewing was approximately 30 min, during which the rad_counts slowly increases by approximately 20 counts (scale factor ~ 35 counts/K) due to receiver gain changes with the receiver physical temperature. A similar pattern is seen in the radiometer output while viewing the cold-sky reflector (shown in dark gray). It is noted that the light and dark gray traces are parallel and offset by about six counts which indicates that the main reflector is biased slightly hot (~ 0.17 K) compared to the cold-sky reference temperature. Similar patterns are seen for all six polarizations at 37 GHz in Fig. 16.

Next, the radiometer output was converted to absolute brightness temperature, using the measured hot-load temperature and assuming that the cold-sky apparent brightness temperature equaled 2.73 K. During the period of maximum pitch $(+45^\circ)$, the main reflector brightness temperature was examined as a function of the azimuth look direction to determine whether or not along-scan Tb biases existed. To improve the measured Tb standard deviation, brightness temperatures were averaged over 2° bins in azimuth. Within these bins, the histograms of Tbs were Gaussian, and results obtained with and without bin averaging were verified to be identical. Results are given for rev-316, at 37 GHz and all polarizations in Fig. 17, where the azimuth is presented as bin numbers (2° bin averages); and the forward direction (360°) corresponds to azimuth bin number 180. For 37 GHz, the measured Tb of space was extremely flat versus azimuth position for the forward look (azimuth positions approximately $\pm 60^\circ$ or azimuth bin numbers 150–210), which indicates negligible scan Tb bias. The increase of Tb at the right-hand edge of the figure indicates feed pattern interception of the hot-load; and these results were used to establish the azimuth range for forward Earth viewing swath. Because 37 GHz uses three different feeds (displaced along an arc from the spin axis) to provide six polarizations, the usable azimuth range for each polarization are slightly different as seen in the various panels of this figure.

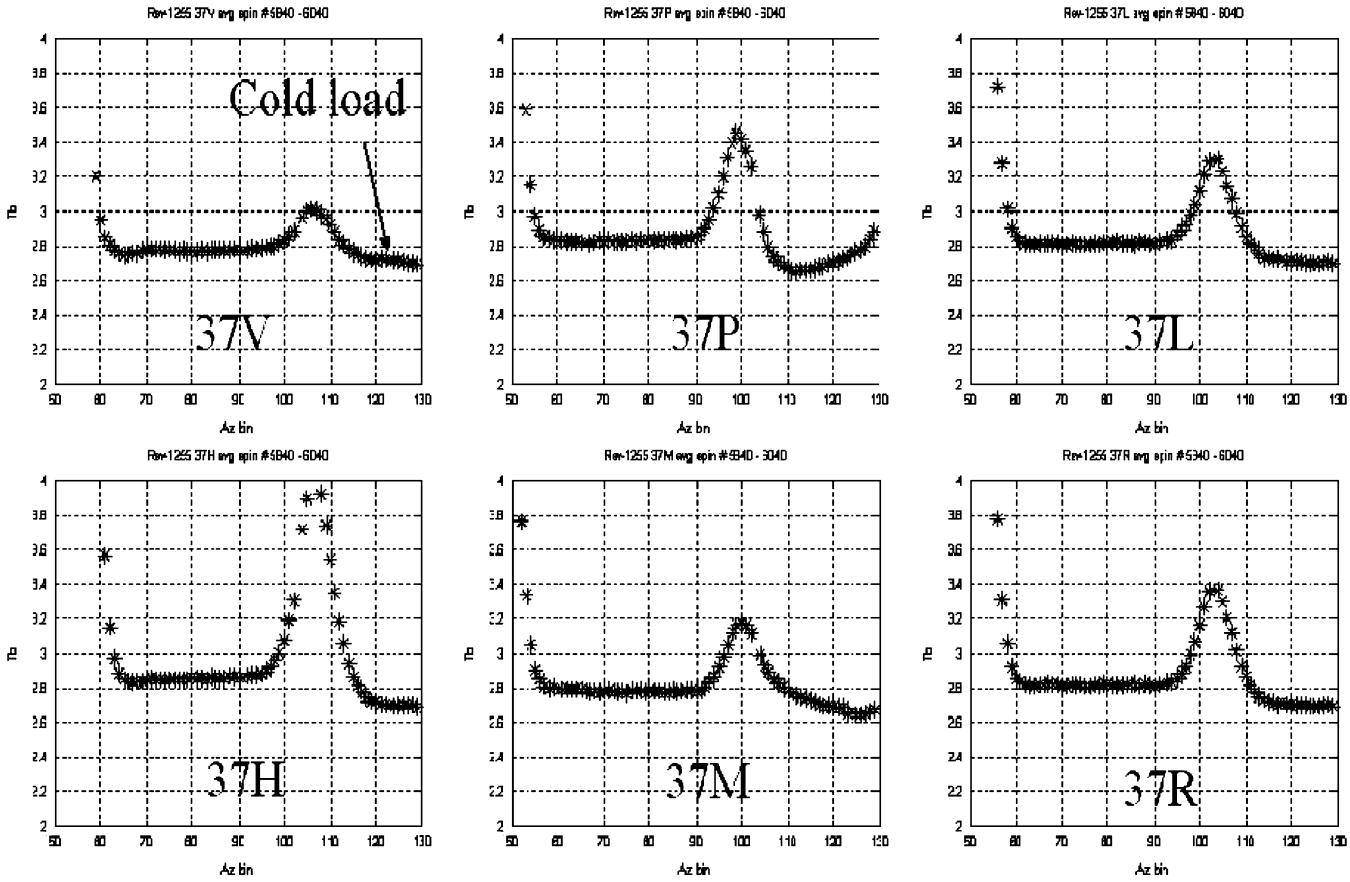

Fig. 20. Measured azimuthal distribution of main and cold-sky reflector Tbs (aft look) during -45° pitch dwell, rev-1255, for 37 GHz all polarizations. The X axis is azimuth bin number (2° steps) where number 90 is an azimuth of 180°.

There were four $+45^\circ$ pitch maneuvers conducted over 15 months, and the repeatability of results was approximately 0.1 K as shown in Fig. 18. This suggests that the long-term calibration stability is better than the prelaunch requirements of 0.58-K bias. Also, similar results were found for the other WindSat channels, which are presented in the Appendix; and a summary of the channel absolute biases (main reflector minus cold-sky calibration) averaged over the forward (and aft) swath azimuth positions and the various pitch maneuvers ($+45$ and -45 pitch) is presented for all channels in Table II.

B. -45° *Pitch Maneuvers*

Companion sets of pitch maneuvers were repeated in the opposite direction (negative pitch) to perform absolute Tb calibration of the main beam over the aft viewing scan. As previously discussed, the aft viewing scan is reduced in width and offset to the left side of the satellite subtrack. Similar results were found for the 37-GHz aft swath comparisons; and results are presented for rev-1255 in Fig. 19 (rad_counts comparison), Fig. 20 (Tb versus azimuth), and Fig. 21 (composite Tb versus azimuth for four revs).

In Fig. 20, the aft azimuth range includes both the main reflector aft scan and the scan over the cold-sky reflector. The best results are shown in the upper right-hand panel for the 37-GHz circular polarized (CP) feed. Of all the WindSat channels, this feed is located closest to the main reflector focal point and produces the best component beam antenna pattern. For this CP feed, the cold-load "sweet spot" (bin number 123) is defined as the azimuth position for the best cold-sky reflector performance (coldest rad_counts) as determined from normal cold calibration measurements (not during pitch maneuver). Note that the sweet spot varies for each feed, and the azimuth location for all 22 channels is presented in Table III. Further, at bin number 105 there is an increase in Tb as the feed transitions from the cold-sky to the main reflector. This increased Tb over this transition region is most likely the result of a significantly distorted antenna pattern (two reflectors simultaneously illuminated by the feed) and resulting sidelobes receiving emissions from the spacecraft/Earth. The aft scan is located from bin numbers 62–93, where the Tb is flat; and the hot-load feed pattern interference is first observed at bin number 60. Also, note that the main reflector is biased hot by a few tenths Kelvin compared to the cold-sky reflector. This is very similar to the corresponding results for the forward scan. Further, composite results presented for the four negative pitch revs: 1255, 1952, 2594, and 4529 show excellent repeatability.

Finally, the Tb differences between orthogonal-polarization channels for the three 37-GHz polarimetric feeds are presented in Fig. 22. These comparisons are very significant, especially for the third and fourth Stokes parameter channels ($\pm 45^\circ$ and LHCP/RHCP), which are very susceptible to Tb biases in either channel. These results are very consistent for both positive

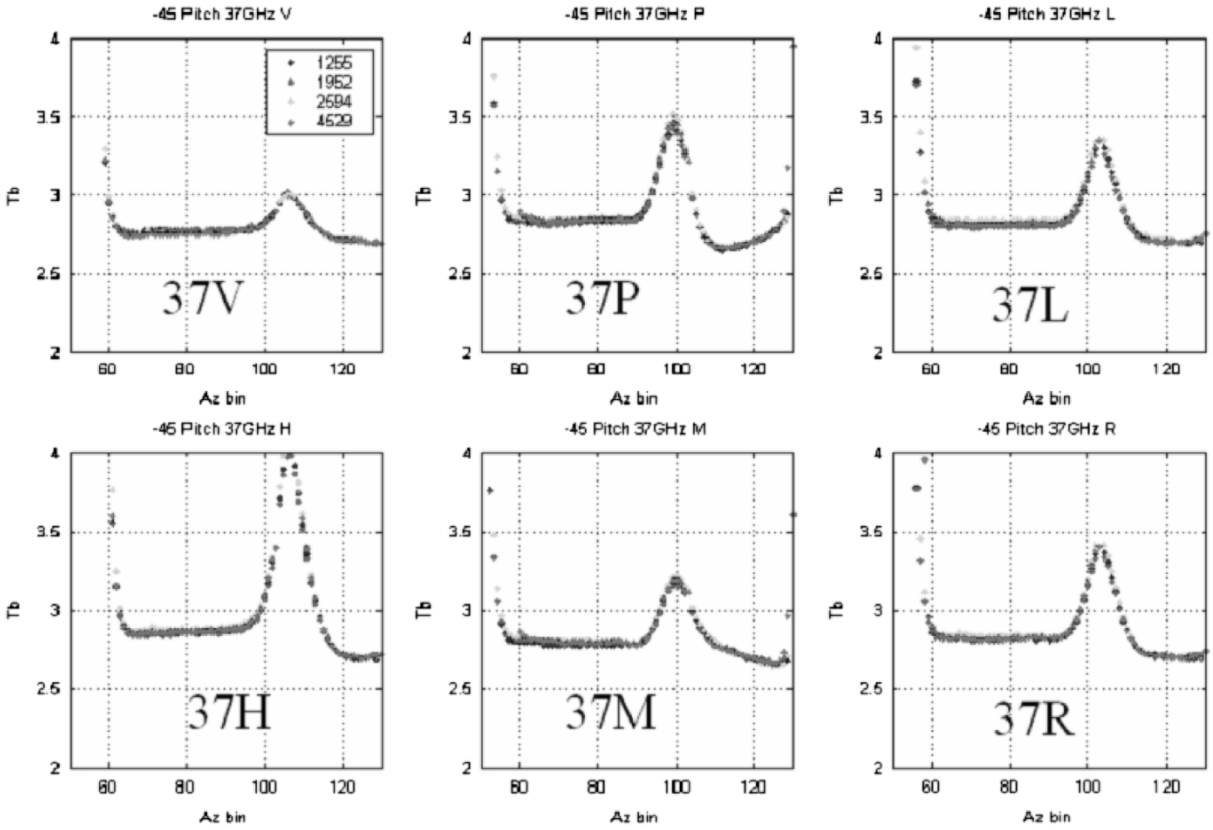

Fig. 21. Composite main and cold-sky reflector Tbs for aft look during -45° pitch dwell for 37 GHz all polarizations for revs: 1255, 1952, 2594, and 4529. The X axis is azimuth bin number (2° steps) where number $90 = 180^\circ$.

and negative pitch revs; and they demonstrate that the orthogonal channels are extremely well matched, such that the average difference of their instantaneous Tbs are nearly 0 K. Thus, no empirical Tb corrections are necessary before applying the antenna pattern corrections in the SDR ground data processor.

These 37-GHz results are representative of those for the other WindSat channels, which are presented in the Appendix. Also, a summary of the channel absolute biases (main reflector minus cold-sky calibration) averaged over the aft (and forward) swath azimuth positions and the various pitch maneuvers (-45 and $+45$ pitch) are presented for 22 channels in Table II.

C. Cold-Calibration Spillover

To assess a potential impact on the WindSat radiometric calibration caused by coupling (spillover) between the main reflector and the 11 feeds (22 channels), an analysis was performed of cold-load brightness temperatures measured under normal operations (satellite in nadir pointing attitude control). During the cold-load measurement, the feed/cold-sky reflector forms a beam that views space; however, the main reflector also simultaneously views the Earth's surface and spillover of the main reflector apparent brightness temperature can occur.

Reliable results were obtained by examining the cold-load counts while the satellite passed over large nearly homogeneous land masses surrounded by ocean, which produced large apparent brightness temperature changes (> 100 K) on the main reflector at the land/ocean boundaries. For this analysis, five passes over Australia and one over South America were selected during the period April–July, 2003. A typical example (rev-2611) is presented in Fig. 14, where ground tracks are shown for the locus of main reflector footprints during the azimuth position corresponding to the cold-sky reflector sweet-spot (light gray trace) and for the closest main reflector measurements (black trace) while viewing forward. During these six orbital passes, rad_count time series were produced for selected azimuth averages (2° bins) corresponding to the cold-sky reflector "sweet-spot" and three nearby azimuth positions (-8°, -12° and -16° offsets), where the feeds illuminated the cold-sky reflector. To estimate the corresponding main reflector rad_counts during the

TABLE III
COLD-SKY REFLECTOR/HOT-LOAD SWEET-SPOT AZIMUTH BIN NUMBER POSITIONS

Freq.	V/H feed	P/M feed	L/R feed
37	Cold =127, hot = 49	119, 41	123, 45
23.8	107, 50	N/A	N/A
18.7	128, 51	118, 40	123, 45
10.7	129, 52	117, 39	123, 45
6.8	105, 30	N/A	N/A

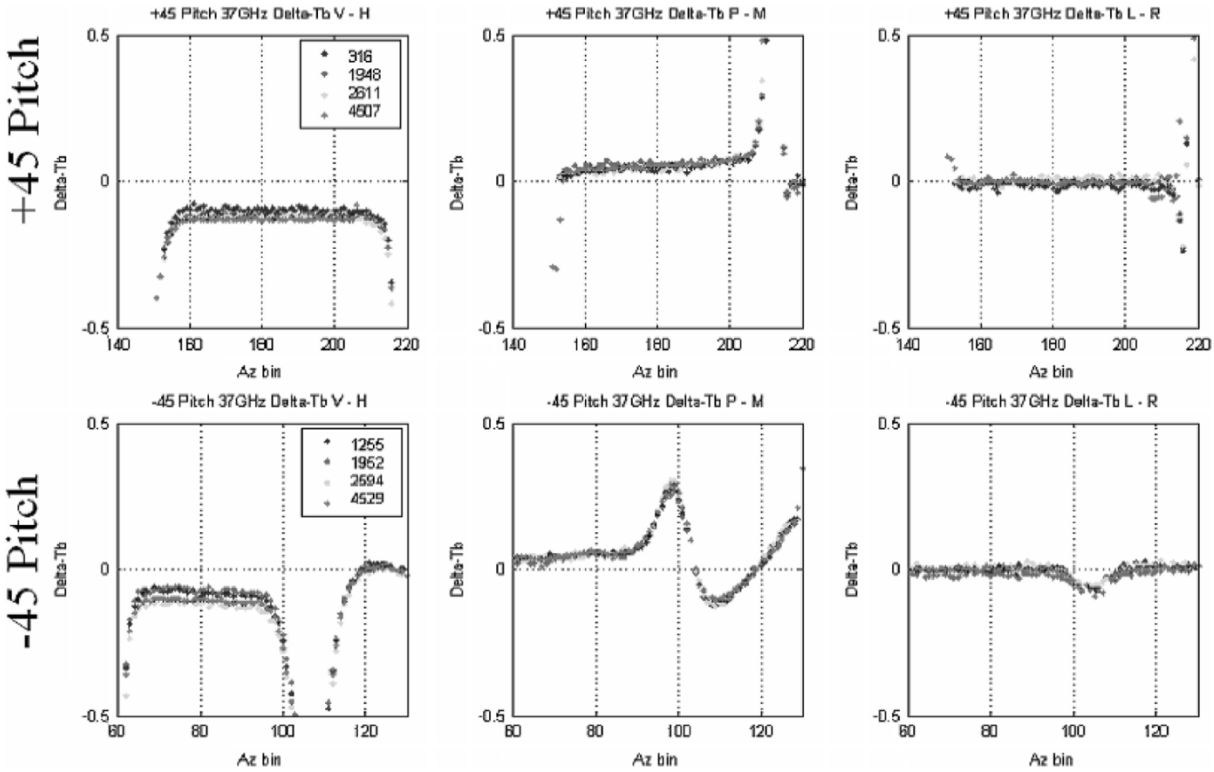

Fig. 22. Differential Tb for orthogonal channels (V-H, P-M, and L-R) during $\pm 45^\circ$ pitch dwell for 37 GHz and for eight revs (four positive pitch in upper panels and four negative pitch in lower). The X axis is azimuth bin number (2° steps).

cold-sky measurement, the main reflector time series was produced for the 2° azimuth bin at the right hand edge of scan while viewing forward. After normalizing for receiver gain drift and adjusting for the time difference in the main reflector and the cold-load measurements, these time series (Fig. 23) were cross-correlated with the main reflector series to establish the spillover coupling.

The effect of main reflector spillover is modeled as an additive rad_counts bias. This corresponds to the sum of emissions from space (through the cold reflector secondary pattern) and the Earth (weighted by the main reflector spillover coupling, R)

$$\text{rad\_counts}_{\text{cold-load}} = \text{rad\_counts}_{\text{cold-reftr}} + R * \text{rad\_counts}_{\text{main-reftr}}. \quad (1)$$

The spillover coupling factor is derived, versus azimuth position, from the cross-correlation of the main reflector rad_counts with the cold-load rad_counts at the various azimuth positions during the cold-load calibration. A linear regression of rad_counts is performed using the main reflector and the four separate azimuth locations during the cold-load measurement.

An example is presented in Fig. 24 as four scatter diagrams of 10.7-GHz P-pol $(+45^\circ)$ cold-sky reflector rad_counts (y axis) versus main reflector rad_counts (x axis) with the resulting linear regression line. Upper-left panel is the azimuth corresponding to the cold-load sweet-spot minus 16°, and upper-right panel is the azimuth corresponding to the cold-load sweet-spot minus 12°. Lower-left panel is the azimuth corresponding to the cold-load sweet-spot minus 8°; and the lower-right panel is the azimuth corresponding to the cold-load sweet-spot. In each panel of the figure, the cluster of points at low rad_counts (lower left) corresponds to the ocean measurements whereas the clusters of points at higher rad_counts (upper right) correspond to land. There is tight grouping of ocean and land points; and for clarity, the transition points between ocean and land have been omitted.

The slope of the linear regression line is the main reflector/feed coupling coefficient (R), which increases with the azimuth offset from the sweet-spot. It should be noted that the slope of the regression curve for the sweet-spot scatter diagram (lower-right panel) is quite small—typically delta-y of only one to three rad_counts. Given that this delta-y is of the same order as the channel precision (least significant bit), the uncertainty increases due to A/D quantization noise for this small coupling value when the coupling (slope) is less than about 1×10^{-3} (-30 dB). Moreover, in a few instances, the scatter of the measurements, due to quantization noise and improper gain normalization, cause the slope of the regression to be negative (a physically impossible outcome). Therefore, to provide a reasonable estimate of the coupling at the sweet-spot, we subjectively edit these data to remove unrealistic values; and then using the remaining points from all cases combined, fit a quadratic curve to the logarithm of the coupling versus azimuth position. From this best fit curve, we estimate the coupling value at the sweet-spot.

For this case (rev-2611), a typical example is shown for the 10-GHz P-pol in Fig. 25, where the coupling value is -34 dB. At this level of spillover coupling and assuming a worst case 300-K Earth brightness, the brightness contribution

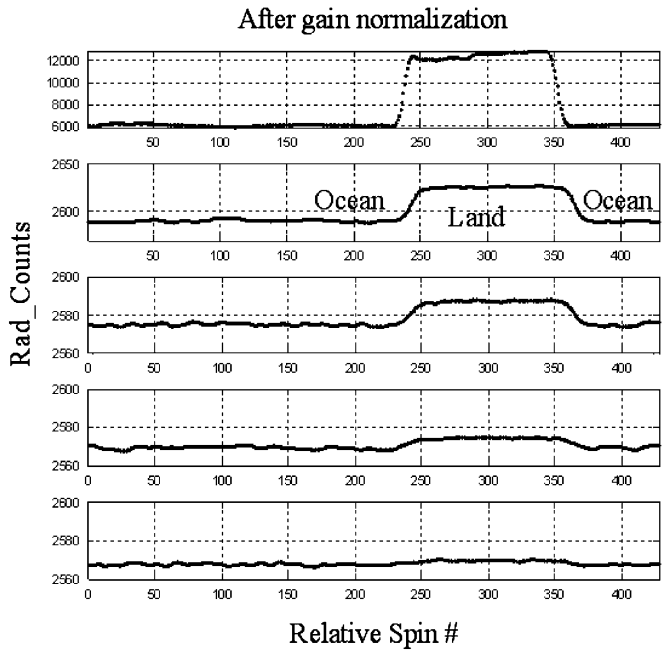

Fig. 23. Time series of rad_counts for 10.7-GHz H-pol during rev-2611. Upper panel is main reflector looking forward at the right-hand edge of swath. Second panel (from top) is the azimuth corresponding to the cold-sky reflector sweet-spot minus 16°. Third panel is the azimuth corresponding to the sweet-spot minus 12°. Fourth is the azimuth corresponding to the cold-load sweet-spot minus 8°. The bottom panel is the azimuth corresponding to the cold-load sweet-spot.

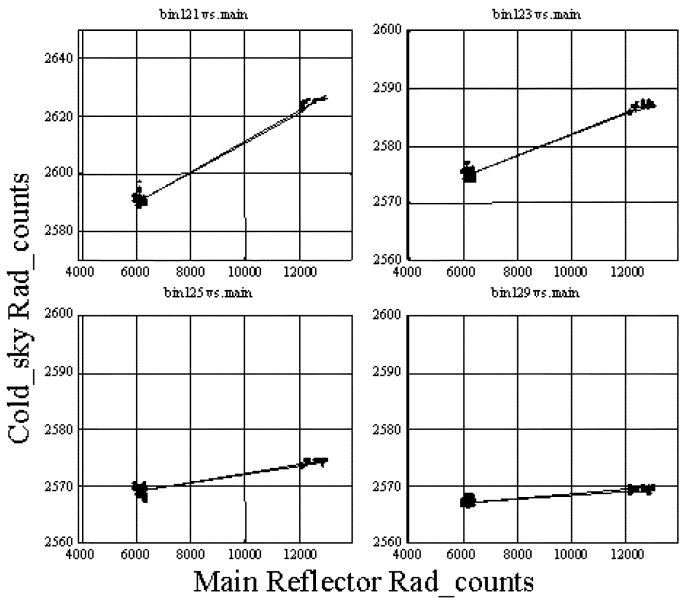

Fig. 24. Example of main reflector spillover determination over Australia, rev-2611. The slope of the linear regression line is the coupling coefficient. Upper left panel is the azimuth corresponding to the cold-sky reflector sweet-spot minus 16°. Upper right is the azimuth corresponding to the sweet-spot minus 12°. Lower left is the azimuth corresponding to the cold-load sweet-spot minus 8°. The lower right is the azimuth corresponding to the cold-load sweet-spot.

from the main reflector is 0.12 K, which is small compared to the measured 2.73-K brightness at the sweet-spot azimuth position. So for this case, the cold-sky Tb is 2.85 K, but the

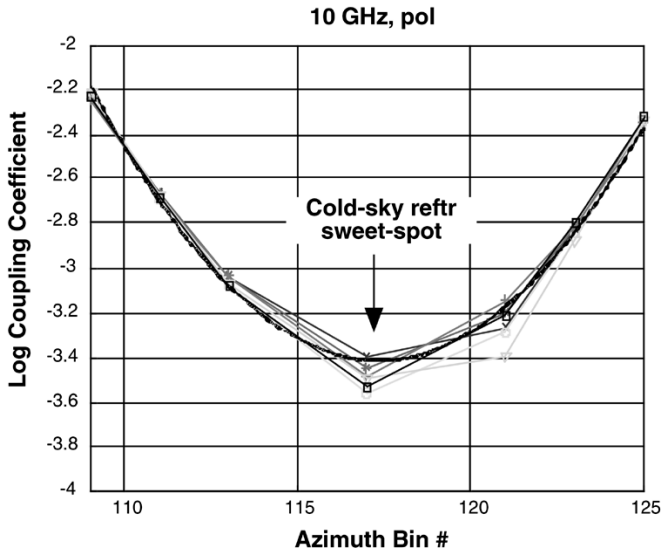

Fig. 25. Typical main reflector spillover coupling (six cases, 10.7 GHz, P-pol). The quadratic best fit curve is shown in bold black.

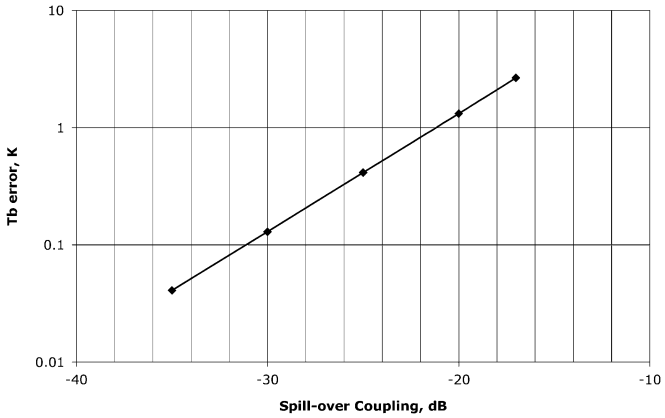

Fig. 26. Tb error introduced by main reflector spillover coupling for a typical ocean scene of 165 K.

TABLE IV
MAIN REFLECTOR SPILLOVER COUPLING COEFFICIENTS

Freq	V	H	P	M	L	R
6.8	2.42E-04	1.71E-04	N/A	N/A	N/A	N/A
10.7	1.74E-04	1.37E-04	2.38E-04	2.17E-04	1.68E-04	1.81E-04
18.7	4.71E-05	1.23E-05	1.01E-04	1.48E-04	3.89E-05	1.45E-05
23.8	4.27E-05	8.62E-04	N/A	N/A	N/A	N/A
37	6.23E-04	3.09E-07	9.75E-05	2.77E-04	6.02E-04	9.38E-05

gain/offset algorithm assumes it to be 2.73 K. However, this error is proportionally reduced as the brightness temperature increases, and at a typical ocean brightness temperature of 165 K the error is $\sim$0.05 K. A plot of ocean Tb error introduced by main reflector spillover is given in Fig. 26. For WindSat, the threshold of concern corresponds to main reflector coupling of -30 dB (1×10^{-3}), which corresponds to 0.13 K. Main reflector coupling analyses were performed for all 22 channels, and results are presented in Table IV. Based upon these

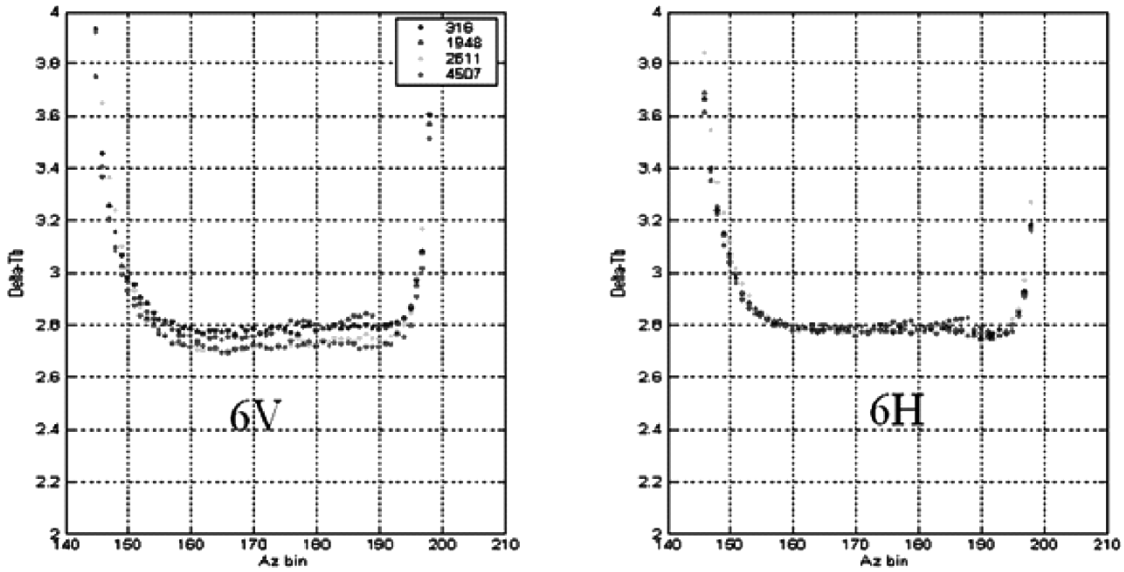

Fig. 27. Measured Tb for main reflector forward look during $+45^\circ$ pitch dwell for 6.8-GHz V- and H- polarizations for revs: 316, 1948, 2611, and 4607. The X axis is azimuth bin number (2° steps) where number $180 = 360^\circ$ and bin number <180 view to the left side of the satellite subtrack and bin number >180 view to the right.

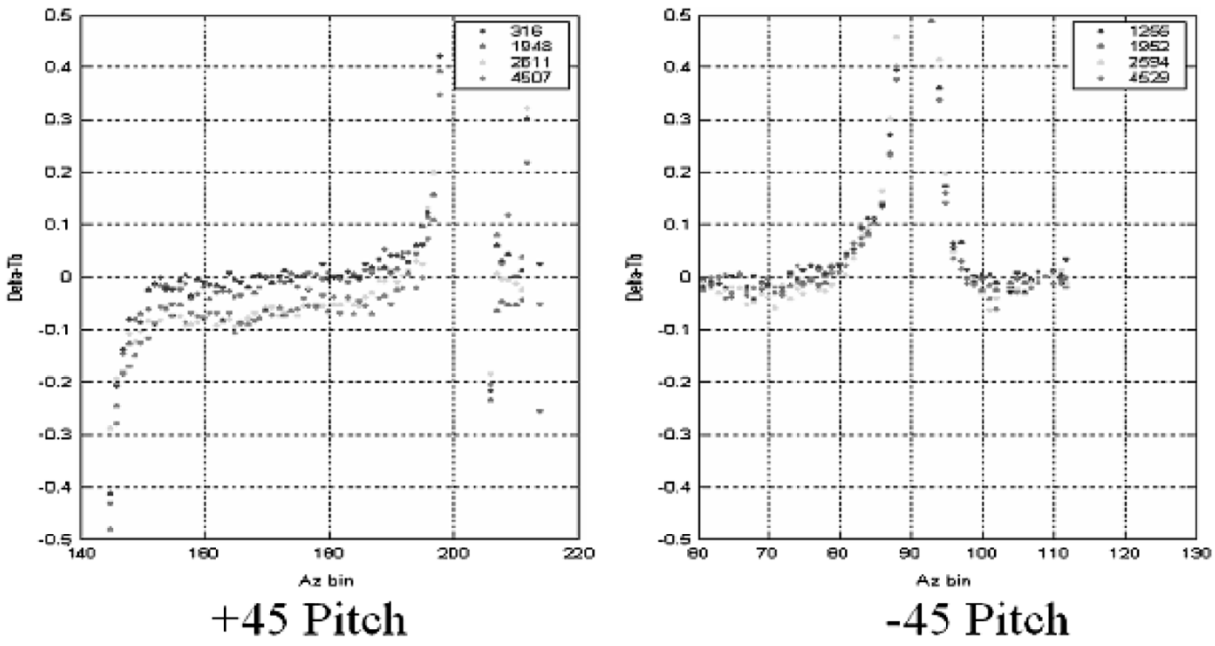

Fig. 28. Differential Tb for orthogonal (V-H) channels during $\pm 45^\circ$ pitch dwell for 6.8 GHz and for eight revs (four positive and four negative pitch). The X axis is azimuth bin number (2° steps).

values, there are negligible radiometric calibration effects for WindSat.

V. Conclusion

The WindSat system presents several unique radiometric calibration challenges because the ocean wind direction signal is two orders of magnitude smaller than the geophysical signals typically measured by passive microwave imagers. As such, the design sensitivity analysis resulted in sensor noise and absolute accuracy requirements approximately 50% tighter than the current SSM/I operational performance. Antenna and receiver polarization purity and horn/antenna/payload alignments are significant elements of the accuracy error budget, and the requirements for radiometric calibration are especially stringent because this is the first polarimetric radiometer to fly in space, and this mission serves as a risk-reduction pathfinder for the polarimetric channels on the future NPOESS CMIS instrument.

This paper focuses on the radiometric calibration requirements for the WindSat polarimetric radiometer and presents results of on-orbit measurements during of a series of special

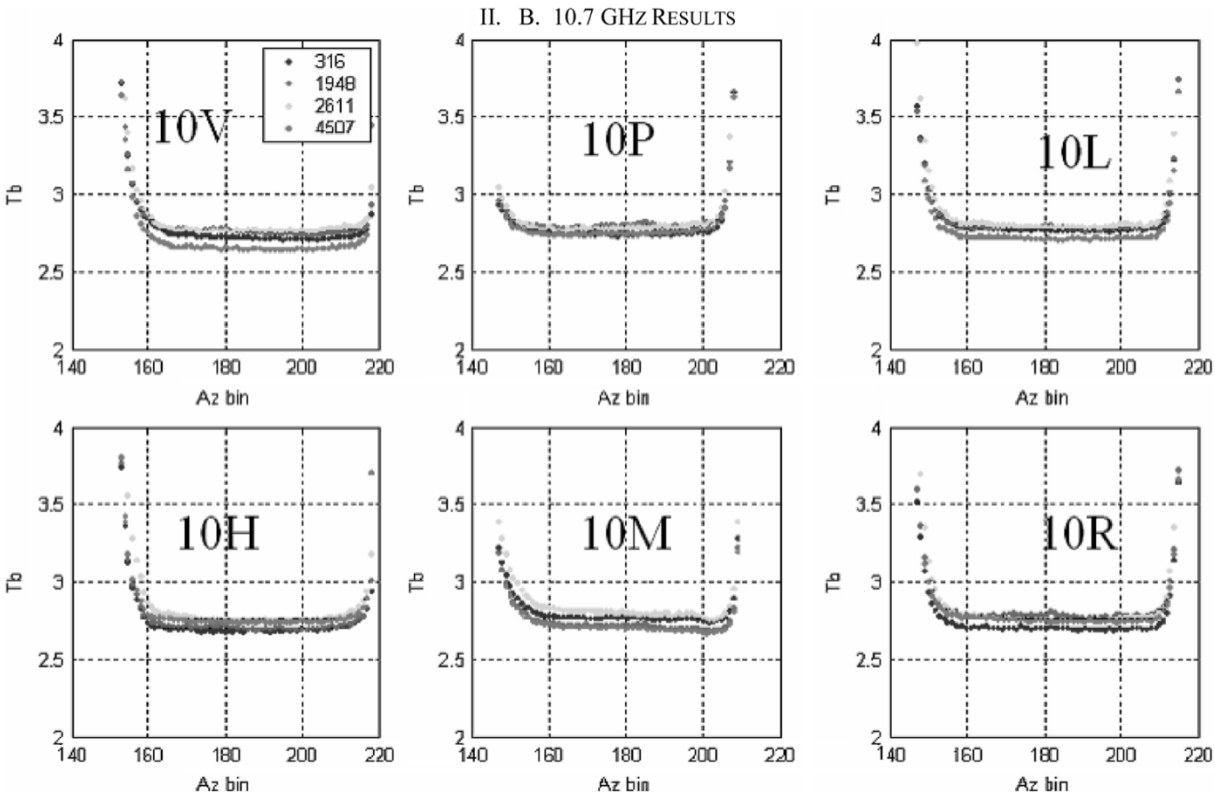

Fig. 29. Measured Tb for main reflector forward look during $+45^\circ$ pitch dwell for 10.7 GHz all polarizations for revs: 316, 1948, 2611, and 4607. The X axis is azimuth bin number (2° steps) where number $180 = 360^\circ$ and bin number <180 view to the left side of the satellite subtrack and bin number > 180 view to the right.

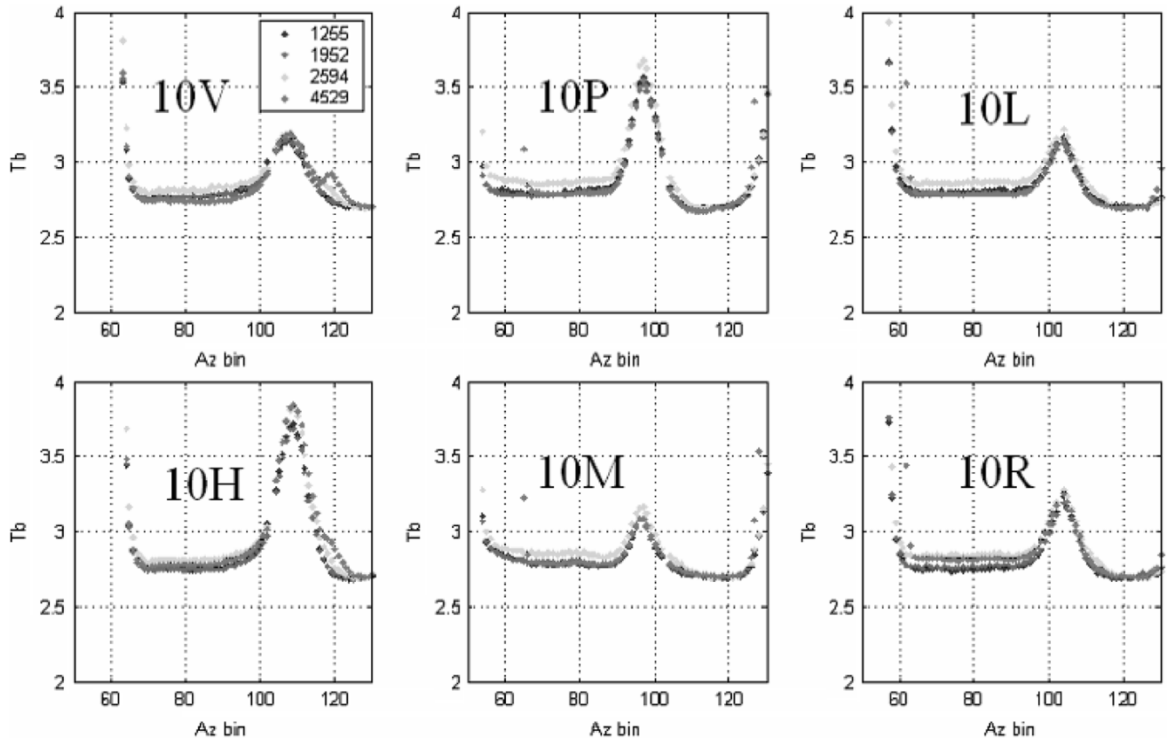

Fig. 30. Measured Tb for main and cold-sky reflectors for aft look during -45° pitch dwell for 10.7 GHz all polarizations for revs: 1255, 1952, 2594, and 4529. The X axis is azimuth bin number (2° steps) where number $90 = 180^\circ$.

satellite pitch maneuvers. Over approximately 15 months, eight radiometric calibration procedures were successfully performed, which verified the excellent long-term calibration stability. These satellite pitch maneuver procedures involved performing brightness temperature measurements, with the instrument in normal operational mode (i.e., antenna spinning

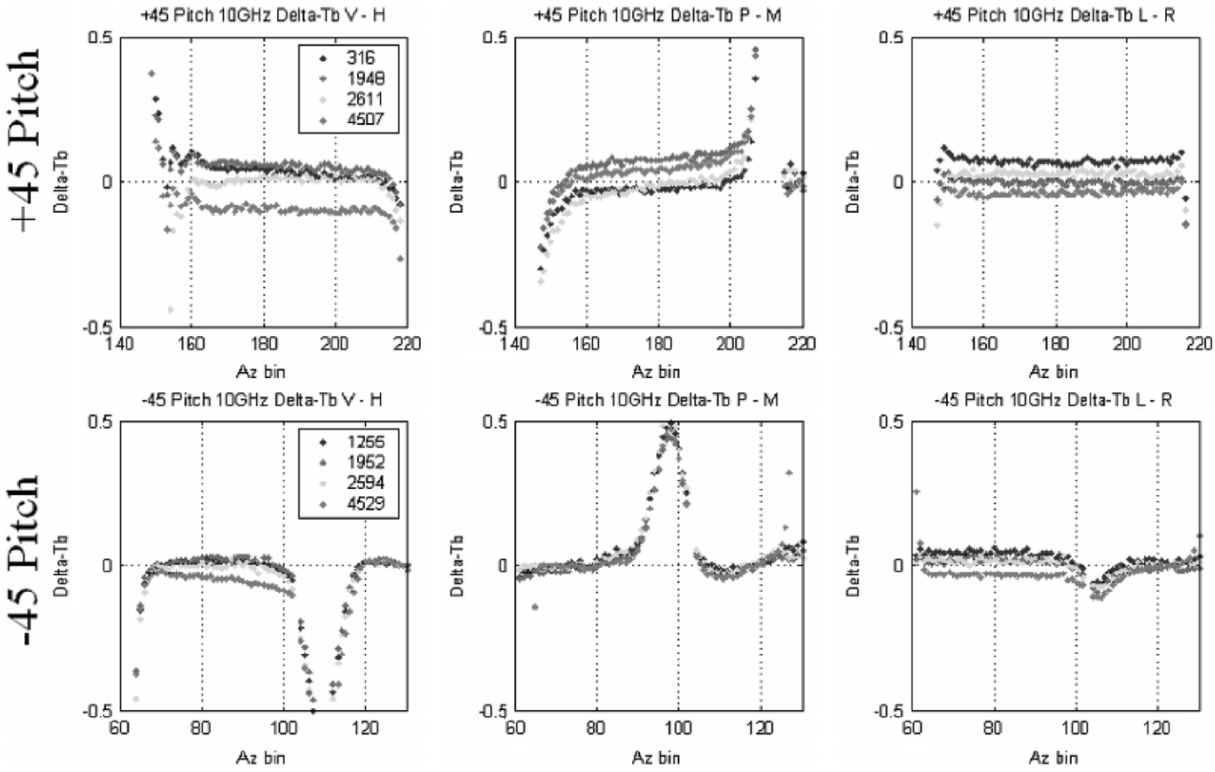

Fig. 31. Differential Tb for orthogonal channels (V-H, P-M, and L-R) during $\pm 45^\circ$ pitch dwell for 10.7 GHz and for eight revs. The X axis is azimuth bin number (2° steps) where number $180 = 360^\circ$ and binnumber $90 = 180^\circ$.

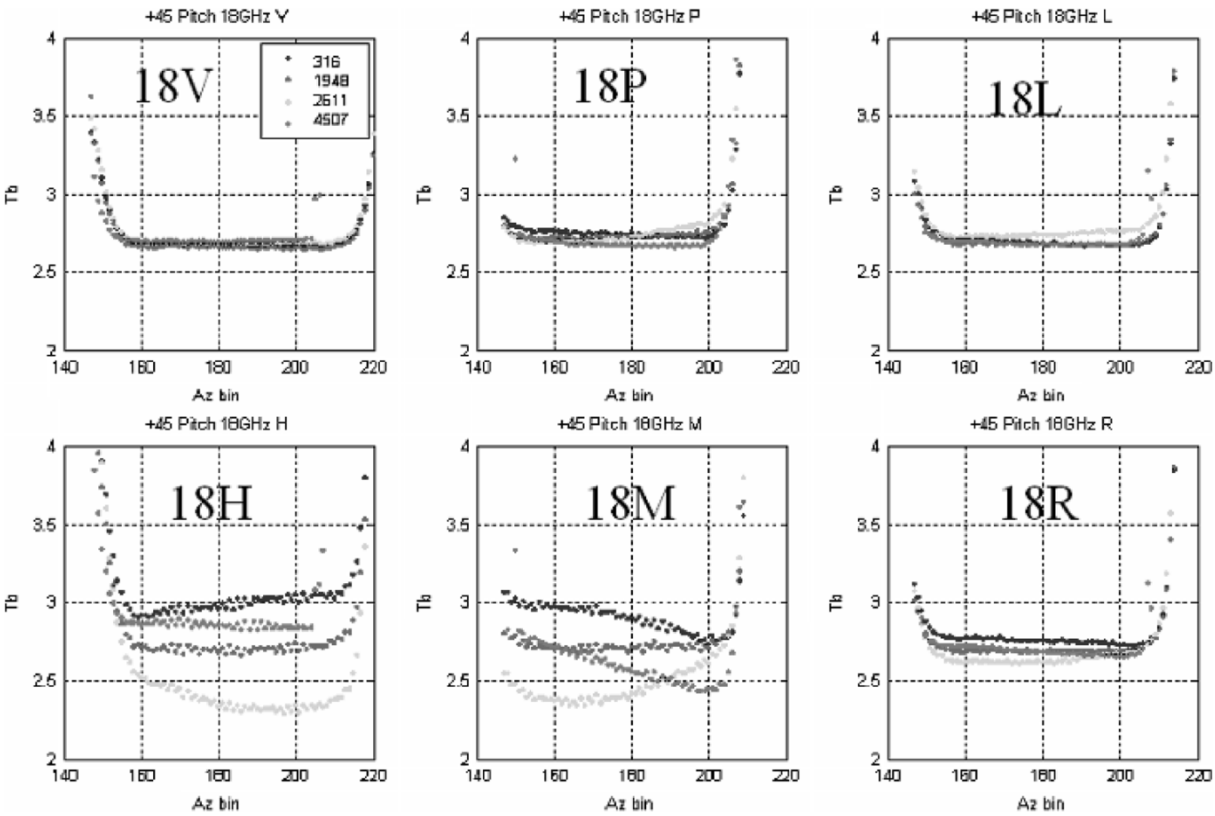

Fig. 32. Measured Tb for main reflector forward look during $+45^\circ$ pitch dwell for 18.7 GHz all polarizations for revs: 316, 1948, 2611, and 4607. The X axis is azimuth bin number (2° steps) where number $180 = 360^\circ$ and bin number < 180 view to the left side of the satellite subtrack and bin number > 180 view to the right.

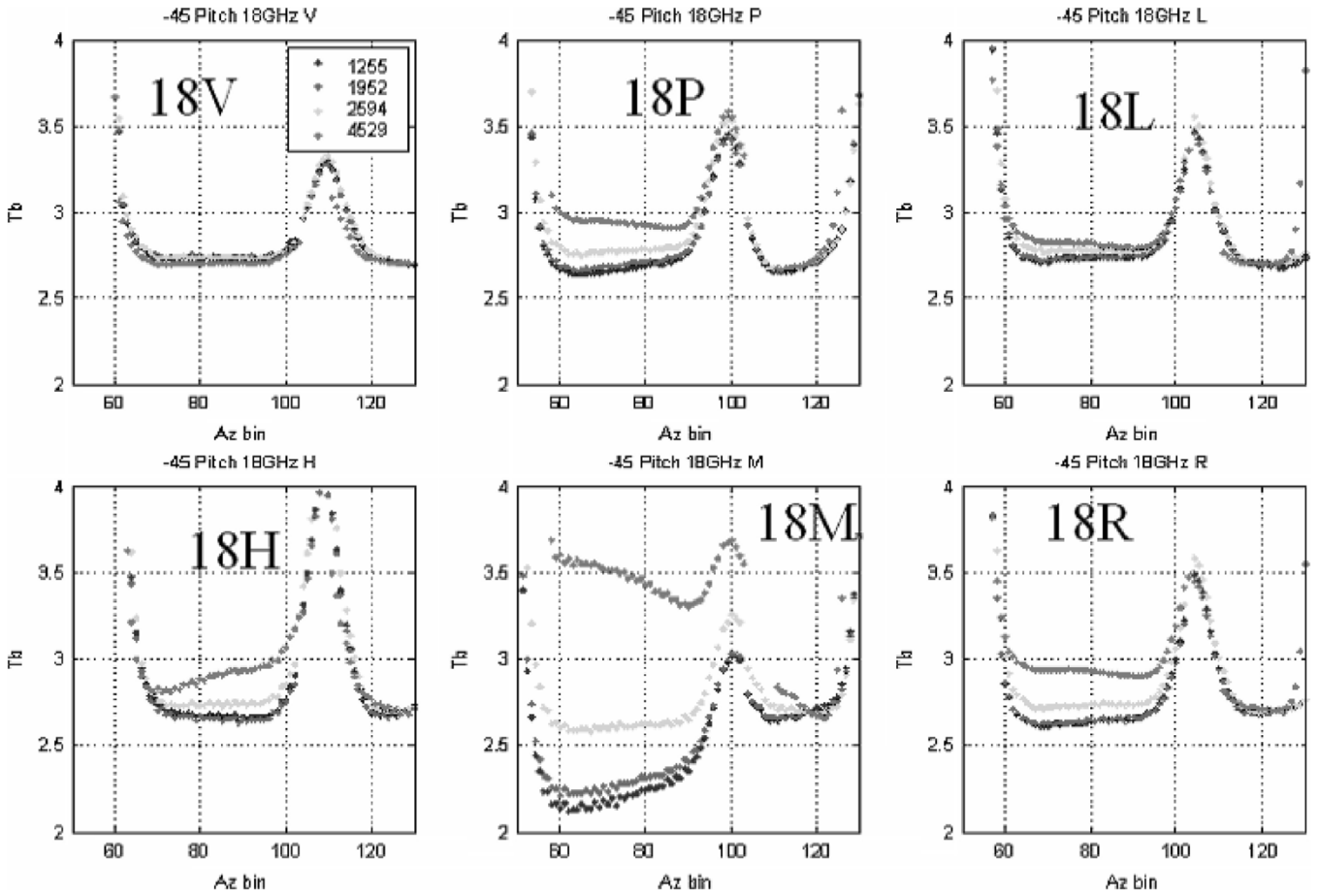

Fig. 33. Measured Tb for main reflector aft look during $-45°$ pitch dwell for 18.7 GHz all polarizations for revs: 1255, 1952, 2594, and 4529. The X axis is azimuth bin number (2° steps) where number $90 = 180°$.

and Tb sampling with both fore and aft viewing), while the satellite's attitude was slowly varied in pitch to cause the antenna beams to point to space where the absolute brightness is a constant 2.73 K. With both positive and negative maneuvers, the main beam viewed space over the full operating azimuth ranges respectively of the forward and aft swaths. When viewing the homogeneous and isotropic brightness of space (uniform 2.73 K), it is possible to determine the absolute calibration of the individual channels and the relative calibration bias between polarimetric channels. For 20 of the 22 channels, the calibration results were extraordinary; but for 18-GHz M-pol $(-45°)$ and H-pol the results were only good. Nevertheless, for all 22 channels these on-orbit tests verified that the WindSat calibration accuracy and radiometer precision exceeds the prelaunch mission radiometric calibration requirements. A summary of key results is presented below.

While viewing the uniform brightness of space, a number of differential Tb measurements were performed and averages (biases) were determined as a function of the azimuth scan position (over 2° bins). Because of the long observation times during a pitch maneuver (∼600 s), the uncertainty effects of the instrument delta-T were eliminated, and the resulting statistical averages were determined with great precision (typically < 0.05 K). Only a few channels had greater uncertainty and these were within a few tenths K, which totally satisfied the prelaunch Tb error budgets. The Tb differences (biases) between the main reflector and the cold-sky reflector for WindSat's channels were typically <0.1 K (max bias $<$ 0.16 K); and the change in absolute calibration with scan position (along-scan biases) were negligible ($<$ 0.1 K) and quite stable over eight pitch maneuvers (four positive pitch and four negative pitch) separated by many months. For the polarimetric channels (V/H, $\pm 45°$ and LHCP/RHCP), the biases between orthogonal channels were small (typically <0.1 K) and very stable over the different pitch maneuvers. Only the 18-GHz $\pm 45°$ channels had greater offsets, which are not believed to be a problem in normal WindSat Tb measurement. Finally, other analyses, conducted to measure the main-reflector Tb coupling into the feeds during the cold-load calibration measurements, were determined to be negligible for all channels.

Thus, the WindSat radiometric calibration campaign is believed to be an outstanding success, and these excellent results provide high confidence in the brightness temperatures from WindSat Temperature Data Records. These results do not include the effects of the antenna pattern correction algorithm, which applies adjustments for cross-coupling between orthogonal polarizations of the channel feed and orthomode transducer. These corrections were determined empirically prelaunch during extensive range calibration, and they are applied in the WindSat SDR product (not reported herein).

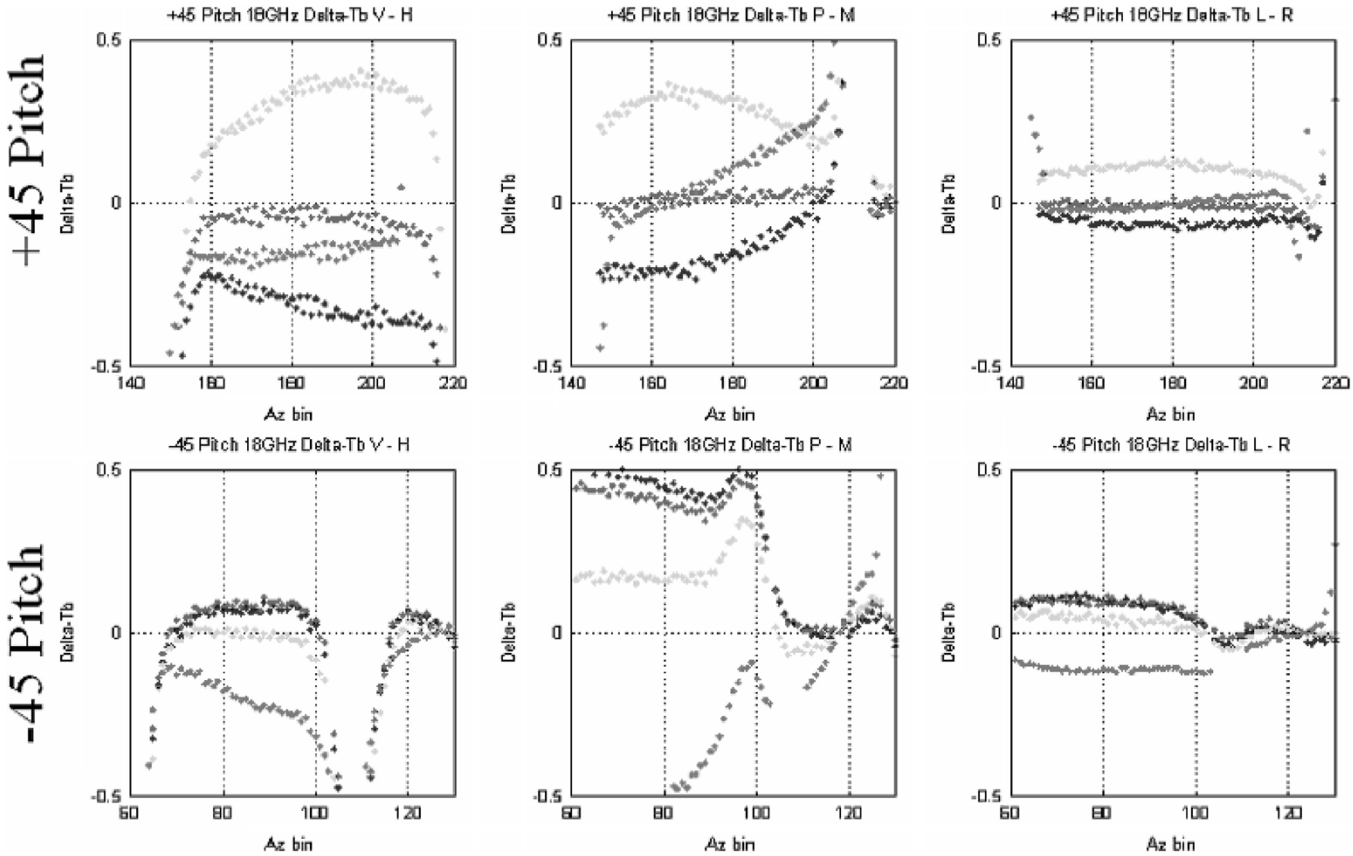

Fig. 34. Differential Tb for orthogonal channels (V-H, P-M, and L-R) during $\pm 45^\circ$ pitch dwell for 18.7 GHz and for eight revs. The X axis is azimuth bin number (2° steps).

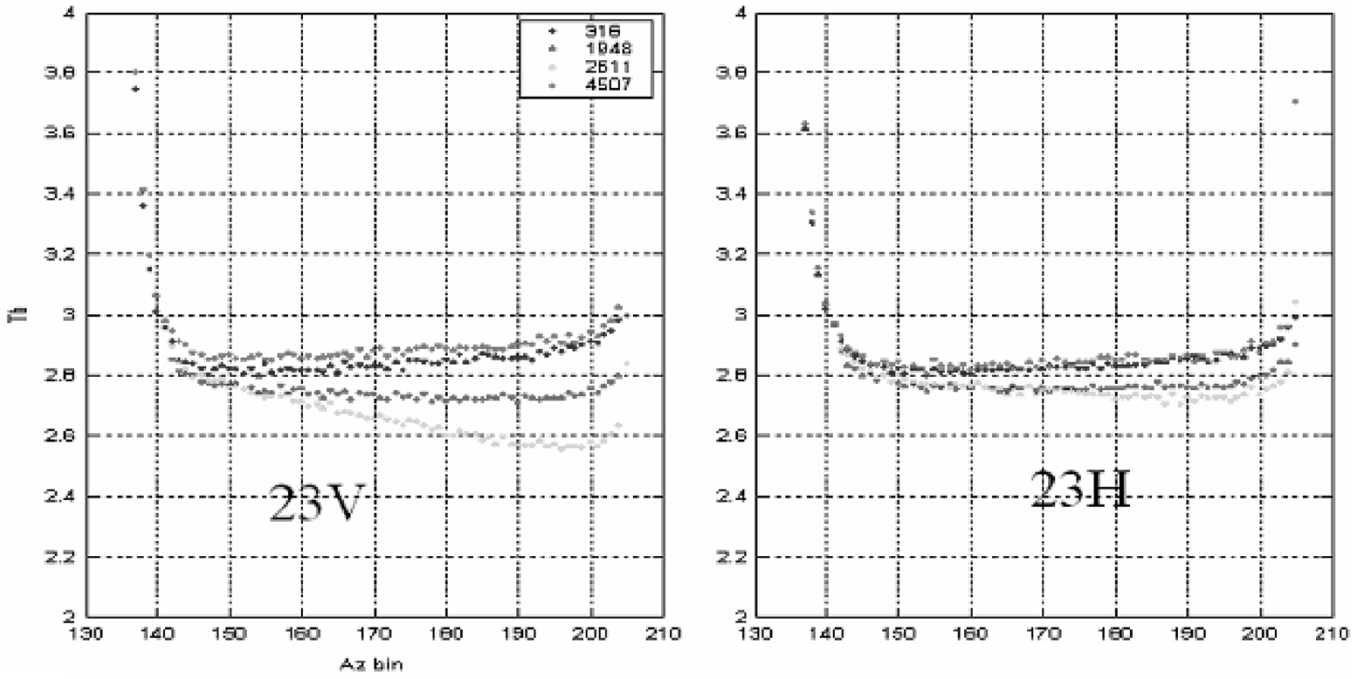

Fig. 35. Measured Tb for main reflector forward look during $+45^\circ$ pitch dwell for 23 GHz for V-pol and H-pol for revs: 316, 1948, 2611, and 4607. The X axis is azimuth bin number (2° steps) where number $180 = 360^\circ$ and bin number < 180 view to the left side of the satellite subtrack and bin number > 180 view to the right.

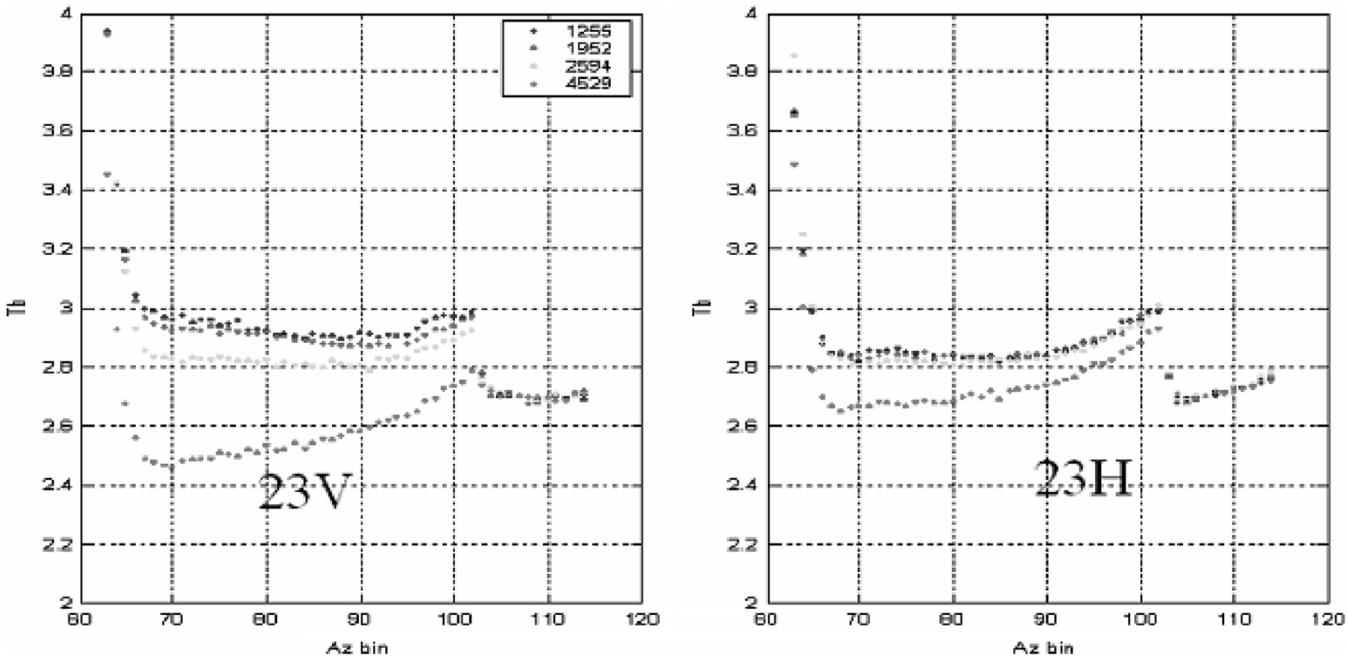

Fig. 36. Measured Tb for main reflector aft look during -45° pitch dwell for 23 GHz for V-pol and H-pol for revs: 1255, 1952, 2594, and 4529. The X axis is azimuth bin number (2° steps) where number $90 = 180^\circ$.

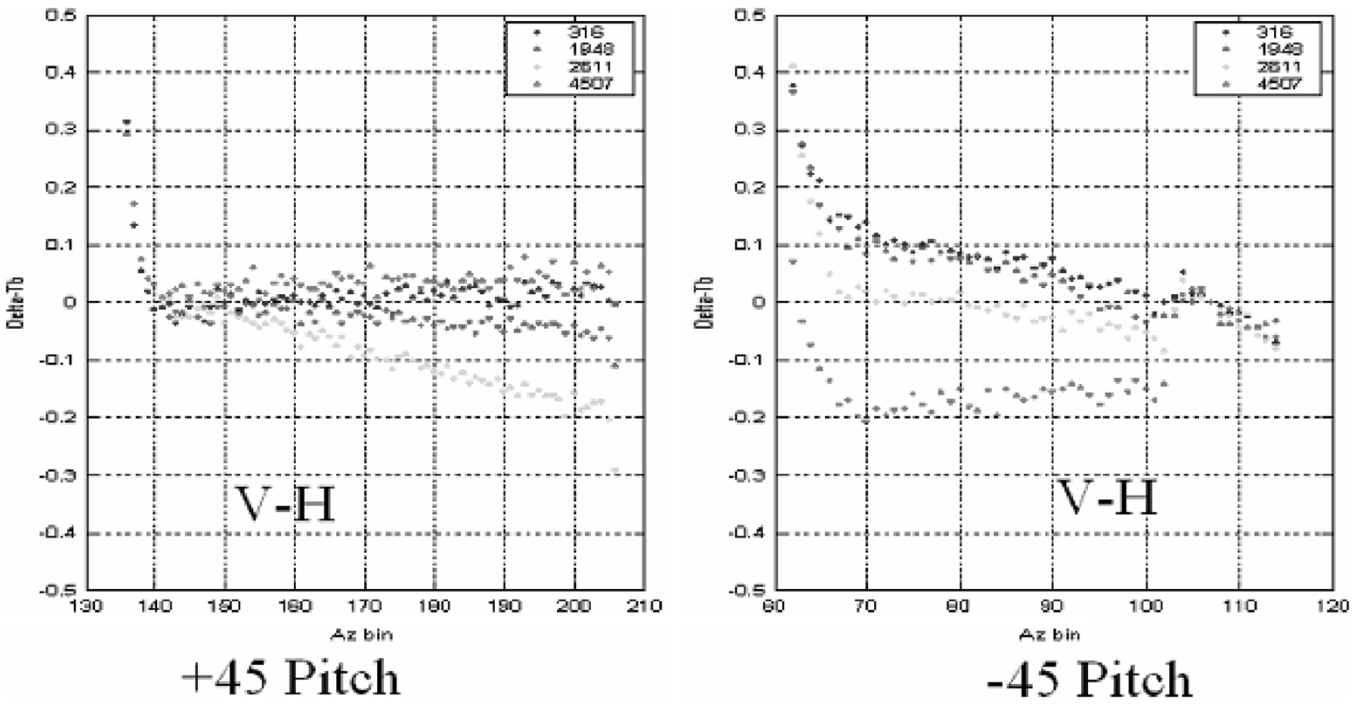

Fig. 37. Differential Tb for orthogonal channels (V-H) during $\pm 45^\circ$ pitch dwell for 23 GHz and for eight revs. The X axis is azimuth bin number (2° steps) where number $180 = 360^\circ$ and binnumber $90 = 180^\circ$.

APPENDIX

This section contains examples of results for the pitch maneuver radiometric calibrations for the remainder (16) of the WindSat channels. The results are presented by frequency in ascending order: 6.8 GHz (Figs. 27 and 28), 10.7 GHz (Figs. 29–31), 18.7 GHz (Figs. 32–34), 23 GHz (Figs. 35–37). The reader is referred to Section IV for a discussion of the figures given for 37 GHz. Except for the frequency, the descriptions are the similar for this material.

REFERENCES

[1] P. W. Gaiser *et al.*, "The WindSat spaceborne polarimetric microwave radiometer: Sensor description and early orbit performance," *IEEE Trans. Geosci. Remote Sens.*, vol. 42, no. 11, pp. 2347–2361, Nov. 2004.

[2] E. M. Twarog, W. E. Purdy, P. W. Gaiser, K. H. Cheung, and B. E. Kelm, "WindSat on-orbit warm load calibration," *IEEE Trans. Geosci. Remote Sens.*, vol. 44, no. 3, pp. 516–529, Mar. 2006.
[3] W. E. Purdy, P. W. Gaiser, G. A. Poe, E. A. Uliana, T. Meissner, and F. J. Wentz, "Geolocation and pointing accuracy analysis for the WindSat sensor," *IEEE Trans. Geosci. Remote Sens.*, vol. 44, no. 3, pp. 496–505, Mar. 2006.
[4] J. P. Hollinger, Ed., "DMSP Special Sensor Microwave Imager calibration/validation," Nav. Res. Lab., Washington, DC, NRL Final Report, vol. 1, Jun. 1989.
[5] W. L. Jones, W. F. Croswell, and D. Ball, "The naval remote ocean satellite system Low Frequency Microwave Radiometer," presented at the *National Radio Science Meeting*, Boulder, CP, Jan. 1987.
[6] F. J. Wentz, P. Ashcroft, and C. Gentemann, "Post-launch calibration of the TRMM Microwave Imager," *IEEE Trans. Geosci. Remote Sens.*, vol. 39, no. 2, pp. 415–422, Feb. 2001.
[7] M. C. Colton and G. A. Poe, "Intersensor calibration of DMSP SSM/I's: F-8 to F-14, 1987-1997," *IEEE Trans. Geosci. Remote Sens.*, vol. 37, no. 1, pp. 418–439, Jan. 1999.
[8] K. Imaoka, Y. Fujimoto, M. Kachi, T. Takeshima, K. Shiomi, H. Mikai, T. Mutoh, M. Yoshikawa, and A. Shibata, "Post-launch calibration and data evaluation of AMSR-E," in *Proc. IGARSS*, vol. 1, Jul. 21–25, 2003, pp. 666–668.

W. Linwood Jones (SM'75–F'99) received the B.S. degree from the Virginia Polytechnic Institute, Blacksburg, the M.E.E. degree from the University of Virginia, Charlottesville, and the Ph.D. degree from the Virginia Polytechnic Institute and State University, in 1962, 1965, and 1971, respectively, all in electrical engineering.

He has over 30 years professional experience with the National Aeronautics and Space Administration (NASA)—Langley Research Center 1962–1981; NASA Headquarters 1988–1992; and the Kennedy Space Center 1992–1994)—and the private aerospace industry—GE Space Division, King of Prussia, PA 1981–1982; Satellite TV Corp., Hightstown, NJ 1982–1984; and Harris Corp., Melbourne, FL 1984–1988. Also, he has over ten years experience in college academia—Florida Institute of Technology, Melbourne, 1994–1996 and the University of Central Florida (UCF), Orlando, 1996–present. At UCF, he is a Professor in the Electrical and Computer Engineering Department, where he teaches undergraduate and graduate courses in satellite communications and remote sensing, and radar systems. Also, he is the Director of the Central Florida Remote Sensing Laboratory, where he performs research in satellite microwave remote sensing. He is a member of the science teams for the Jet Propulsion Laboratory's SeaWinds Scatterometer Program, the NASA Goddard Space Flight Center's Precipitation Measuring Mission, and the Naval Research Laboratory's WindSat Mission.

Dr. Jones is a member of the Union of Radio Scientists International, Commission-F, the American Geophysical Union, the IEEE Geoscience and Remote Sensing Society, the IEEE Antennas and Propagation Society, and the IEEE Ocean Engineering Society.

Jun D. Park (S'92) received the B.S. degree from Konkuk University, Seoul, Korea, and the M.S. degree from the Florida Institute of Technology, Melbourne, both in electrical engineering, in 1993 and 1996, respectively.

He was a Research Associate in Central Florida Remote Sensing Laboratory, University of Central Florida, Orlando from 1996 to 2005 and is currently a Satellite Communication Systems Engineer with Northrop Grumman Mission Systems, Winter Park, FL.

Seubson Soisuvarn (S'02) received the B.Eng. degree from Kasetsart University, Bangkok, Thailand, and the M.S. degree from the University of Central Florida (UCF), Orlando, both in electrical engineering, in 1998 and 2001, respectively, where he is currently pursuing the Ph.D. degree also in electrical engineering.

He joined the Central Florida Remote Sensing Laboratory, UCF, in 2001. His current research interests are measurements of ocean surface wind vectors using active and passive microwave sensing from a satellite.

Liang Hong (S'03) received the B.S. degree in electronic engineering from Tsinghua University, Beijing, China, the M.S. degree in cartography and geographic information systems from the Chinese Academy of Sciences, Beijing, and the M.S. degree in electrical engineering from the University of Central Florida (UCF), Orlando, in 1999, 2002, and 2004, respectively. He is currently pursuing the Ph.D. degree at UCF.

His research interests are in satellite remote sensing, satellite communication, and high-frequency radio wave propagation areas.

Peter W. Gaiser (S'91–M'93–SM'04) received the B.S. degree in electrical engineering from Virginia Polytechnic Institute and State University, Blacksburg, in 1987, and the Ph.D. degree from the University of Massachusetts, Amherst, in 1993, where he studied microwave remote sensing, with emphasis on synthetic aperture interferometric radiometry.

He has been with the Naval Research Laboratory (NRL), Washington, DC, since 1993, and currently Acting Head of the Remote Sensing Physics Branch, Remote Sensing Division at NRL. While at NRL, he has been involved in polarimetric radiometry research. His research interests also include instrument design, data collection, and model development specifically for the purpose of ocean wind vector measurements from space. He is the Principal Investigator for the WindSat spaceborne polarimetric microwave radiometer demonstration project.

Karen M. St. Germain (S'88–M'91–SM'03) received the B.S. degree in electrical engineering from Union College, Schenectady, NY, and the Ph.D. degree from the University of Massachusetts, Amherst, in 1987 and 1993, respectively.

From 1987 to 1993, she was a Research Assistant in the Microwave Remote Sensing Laboratory, University of Massachusetts, where her doctoral research focused on passive microwave remote sensing of oceans and ice. In 1993, she joined the Faculty of the Department of Electrical Engineering, University of Nebraska, Lincoln. While at the University of Nebraska, she taught courses in electromagnetics, signal processing, and radar system design, and expanded her research interests to include passive and active remote sensing of vegetation and soil moisture. In 1996, she left the University of Nebraska to take a position at the Naval Research Laboratory, Washington DC, where she is currently involved in remote sensing system development, spaceborne demonstration of remote sensing concepts, instrument calibration, radiative transfer theory, and algorithm development.

Dr. St. Germain has been a member of the IEEE Geoscience and Remote Sensing Society (GRSS) since 1988. She served as an Associate Editor of the IEEE GRSS Newsletter from 1994 to 1996 and was elected to the GRSS AdCom in 1997. She served as the Membership Chairman from 1997 to 1998 and has served as the Vice President for Meetings and Symposia from 1998 to 2003. She is currently Vice President of Operations and Finance. She was Co-Chairman of the Technical Program for IGARSS 2000 and is a member of Eta Kappa Nu and Tau Beta Pi. She currently serves on the U.S. National Research Council's Committee on Radio Frequencies (CORF).